REVIEW ARTICLE

Rotation and momentum transport in tokamaks and helical systems

View the article online for updates and enhancements.

Review Article

Rotation and momentum transport in tokamaks and helical systems

K. Ida[1] and J.E. Rice[2]

[1] National Institute for Fusion Science, Toki, Gifu 509-5292, Japan
[2] Plasma Science and Fusion Center, MIT, Cambridge, MA, 02139, USA

E-mail: ida@nifs.ac.jp

Abstract

Poloidal and toroidal rotation has been recognized to play an important role in heat transport and magnetohydrodynamic (MHD) stability in tokamaks and helical systems. It is well known that the $E \times B$ shear due to poloidal and toroidal flow suppresses turbulence in the plasma and contributes to the improvement of heat and particle transport, while toroidal rotation helps one to stabilize MHD instabilities such as resistive wall modes and neoclassical tearing mode. Therefore, understanding the role of momentum transport in determining plasma rotation is crucial in toroidal discharges, both in tokamaks and helical systems. In this review paper, the driving and damping mechanisms of poloidal and toroidal rotation are outlined. Driving torque due to neutral beam injection and radio-frequency waves, and damping due to parallel viscosity and neoclassical toroidal viscosity (NTV) are described. Regarding momentum transport, the radial flux of momentum has diffusive and non-diffusive (ND) terms, and experimental investigations of these are discussed. The magnitude of the diffusive term of momentum transport is expressed as a coefficient of viscous diffusivity. The ratio of the viscous diffusivity to the thermal diffusivity (Prandtl number) is one of the interesting parameters in plasma physics. It is typically close to unity, but sometimes can deviate significantly depending on the turbulent state. The ND terms have two categories: one is the so-called momentum pinch, whose magnitude is proportional to (or at least depends on) the velocity itself, and the other is an off-diagonal term in which the magnitude is proportional to (or at least depends on) the temperature or/and pressure gradient, independent of the velocity or its gradient. The former has no sign dependence; rotation due to the momentum pinch does not depend on the sign of the rotation itself, whether it is parallel to the plasma current (co-direction) or anti-parallel to the plasma current (counter-direction). In contrast, the latter has a sign dependence; the rotation due to the off-diagonal residual term is either in the co- or counter-direction depending on the turbulence state, but not on the sign of the rotation itself. This residual term can also act as a momentum source for intrinsic rotation. The experimental results of investigations of these ND terms are described. Finally the current understanding of the mechanisms behind the ND terms in momentum transport, and predictions of intrinsic rotation driven by these terms are reviewed.

Keywords: spontaneous rotation, intrinsic torque, Reynolds stress, residual stress, non-diffusive momentum transport, tokamak, helical system

(Some figures may appear in colour only in the online journal)

1. Introduction

Plasma rotation and momentum transport have been recognized to be important since the role of flow shear ($E \times B$ flow shear) in turbulence suppression was found in H-mode plasmas [1, 2], where a significant reduction of heat transport, and hence an improvement of confinement, is realized. Before the discovery of H-mode [3], the importance of plasma rotation and the radial electric field were not discussed because the impact of rotation on transport was not clearly observed in L-mode plasmas [4]. The suppression of turbulence due to sheared flow through the decorrelation process was proposed as a possible mechanism for confinement improvement in H-mode plasmas [5]. Since the sheared flow perpendicular to the magnetic field is responsible for the decorrelation process, poloidal flow shear, which is often the dominant term of $E \times B$ shear, has been the main focus. However, toroidal flow shear can also be important when it becomes large enough to contribute to the $E \times B$ shear, as demonstrated in VH-mode.

Plasma rotation also contributes to the stabilization of some magnetohydrodynamic (MHD) instabilities. Sustained stabilization of the resistive wall mode (RWM) by plasma rotation has been demonstrated, where the normalized plasma pressure significantly exceeded the free-boundary stability

limit [6]. After the role of plasma rotation in the stabilization of RWMs was clarified [7, 8], the understanding of plasma rotation and momentum transport has been considered to be an essential issue both in heat and particle transport, and in MHD stability.

Because of spontaneous/intrinsic rotation (rotation not driven by applying external torque), momentum transport cannot be expressed with a simple diffusivity, which is usually adapted in heat transport analysis. The existence of spontaneous/intrinsic rotation clearly shows that there is a non-diffusive (ND) term of momentum transport, because a simple solution of $\nabla v_\phi = 0$ (and $v_\phi = 0$ for zero velocity boundary condition) is not possible in the diffusive model when there is no torque input under steady-state conditions.

There are several studies of momentum transport focusing on spontaneous rotation [9] in tokamak experiments, the momentum pinch [10–12], accretion [13], off-diagonal terms of the transport matrix and residual stress [14, 15] from the theoretical point of view. Although spontaneous rotation and its driving mechanism have been highlighted recently, there are other important elements of momentum transport, for example, damping and driving by neoclassical toroidal viscosity (NTV) and wave particle interactions. Since toroidal rotation is not independent of poloidal rotation, the coupling between the two is also important, which depends on the symmetry of the magnetic field configuration (toroidal symmetry is broken in helical plasmas and in plasmas with perturbation fields even in tokamaks). It is important to understand momentum transport in plasmas with various magnetic field configurations. In this paper, diffusive and ND momentum transport, both in tokamaks and helical systems, is reviewed. In section 2, the terms driven by neutral beams, radio frequency (RF) waves and electron cyclotron heating (ECH), and damping by neoclassical parallel viscosity and toroidal viscosity are presented. In section 3, the Reynolds stress, including the diffusive, pinch and residual stress terms, is reviewed. In section 4, interesting features and physics issues for future study are discussed, followed by predictions of intrinsic rotation in section 5.

1.1. Momentum transport

Momentum transport has been recognized to be much more complicated than heat and particle transport in toroidal plasmas. There are several reasons for the complexity of momentum transport. Although the flows in the plasma are vectors, toroidal flow is treated like a scalar quantity. Because flows are divergence free, toroidal flow is not independent of poloidal flow. In general, the magnetic field is tilted in the toroidal direction, and the toroidal flow is not independent of the $E \times B$ flow either.

In axi-symmetric plasmas, the toroidal and poloidal flows have been simplified as follows. The toroidal flow, $V_\phi = \omega_\phi(\psi)R$, where ψ is the magnetic flux and R is the major radius, and V_ϕ profiles are determined by the radial diffusion of toroidal momentum by viscosity perpendicular to magnetic flux surfaces. However, the assumption of 'rigid rotation' (i.e. angular rotation that is a flux function) is only appropriate when the neoclassical effect can be neglected due to the large aspect ratio limit, the small poloidal rotation in L-mode and the large toroidal velocity driven by the strong toroidal torque from

neutral beams, because the toroidal rotation is governed by the radial force balance, and is a function of poloidal rotation, the pressure gradient and the radial electric field, as discussed later in section 1.3. In contrast, the poloidal flow, V_θ, is damped by the friction between the poloidally passing and trapped particles (parallel viscosity), and is determined by the ion temperature gradient (ITG). In non-axi-symmetric plasmas such as in helical devices or tokamaks with perturbed magnetic fields which break the toroidal symmetry, both the toroidal and poloidal flow deviate far from this simple picture. This feature has been recognized as an effect of NTV.

A second important aspect of momentum transport is that there are various toroidal torques in the plasma because of the existence of strong magnetic fields. In plasmas with tangential neutral beam injection (NBI), the collisional momentum torque supplied by collisions between the beam ions and the bulk plasma is dominant, and momentum transport has been studied by assuming a simple radial diffusion process of toroidal momentum. The toroidal flow driven by the $j \times B$ force due to fast ions has been found to be important. Although the importance of this effect was pointed out in the early 1980s [16], the driving mechanism has been studied experimentally only in helical plasmas. More recently the importance of this driving mechanism due to fast ions from neutral beams or excited by ion-cyclotron range of frequency (ICRF) waves has been recognized in tokamak experiments. These various driving mechanisms, which have not been included in momentum transport, were found to be important.

The third important aspect of momentum transport arises from the ND terms. It is well known that there is an intrinsic flow, even in plasmas without external collisional momentum input, such as in ohmic, ICRF, ECH or lower hybrid current drive (LHCD) discharges. Because of the complexity, the mechanisms are not clear. However, there are several experiments which clearly show the ND nature of momentum transport. The existence of ND terms is an important finding because it predicts significant toroidal flow required for the MHD stability without external collisional momentum input. However, a deep understanding of the mechanisms of the ND terms is necessary for a more accurate prediction of the toroidal flow.

Figure 1 shows a diagram of the terms which contribute to momentum transport. There are various driving and damping mechanisms. These forces are balanced with the Reynolds stress, which underlies the physics mechanism of radial transfer of angular momentum. Because of the conservation of the angular momentum, the Reynolds stress does not produce net rotation, unless the angular momentum is released from the core plasma to the scrape-off layer plasma through the last closed flux surface (LCFS). However, the Reynolds stress may produce a net rotation for the given species by the turbulence acceleration terms, because the conservation of the angular momentum is in the total (summed over all species) momentum, not in the momentum for a given species. This effect could be one of the mechanisms causing the discrepancy between the measurements and predicted neoclassical values for toroidal rotation among different species, as described later in this review. The momentum flux due to the Reynolds stress can be expressed as three terms; a diffusive term due to viscosity, a term proportional to the toroidal rotation
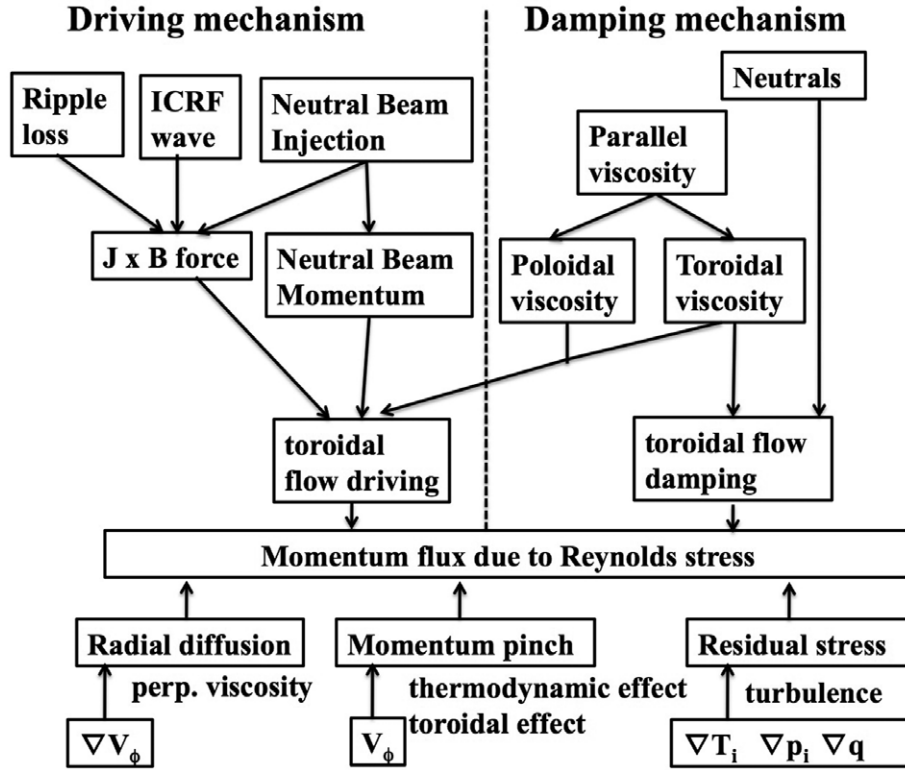
Figure 1. Diagram of essential elements of the toroidal momentum transport.

velocity, and a residual stress which does not explicitly depend on the velocity gradient and velocity itself. The term proportional to the toroidal rotation velocity is called the momentum pinch term and there are several theoretical models based on thermodynamic [17] and toroidal effects (turbulent equipartition (TEP) the Coriolis force).

By including the ND term of the momentum flux as an off-diagonal term between momentum and heat fluxes, the radial flux of toroidal momentum, P_ϕ, can be written as

$$P_\phi(r) = \frac{1}{r} \int_0^r r' \left(T(r') - \frac{d[m_i n_i(r')V_\phi(r')]}{dt} \right) dr', \quad (1)$$

which can be calculated by integrating the toroidal torque, T, inside the magnetic flux surface.

$$T = T_M + T_{j \times B} + T_{vis} - T_{n_0}, \quad (2)$$

where $T_M(r)$ is the torque due to the collisional damping of the fast ions from the neutral beam, while $T_{j \times B}$ is the torque due to the Lorentz $j \times B$ force of radial current and poloidal magnetic field. T_{vis} and T_{n_0} are the viscosity and damping forces due to collisions with neutral particles. It should be noted that the viscosity force can be a driving or damping term for toroidal rotation. Since the rotation velocity and torque have signs defined as positive for the co-direction (parallel to the plasma current) and negative for the counter-direction (anti-parallel to the plasma current), a positive torque increases the co-rotation but decreases the counter-rotation. The torque which is not directly connected to the toroidal velocity is considered to be a true torque, while the torque which is directly connected (roughly proportional to the toroidal velocity itself)

is considered to be a damping term. There are several driving torques which are categorized as collisional toroidal torques, such as due to tangentially injected neutral beams, and the $j_r \times B_\theta$ torque, where j is the non-ambipolar radial flux due to the bulk plasma in non-axi-symmetric discharges, or due to fast ions from neutral beams or excited by ICRF waves in tokamaks.

The radial flux of toroidal momentum is balanced by the turbulence-driven flux as [18]

$$P_\phi(r) = \underbrace{m_i v_\phi(r) \langle \tilde{v}_r \tilde{n}_i \rangle}_{\text{convective flux}} + \underbrace{m_i n_i(r) \langle \tilde{v}_r \tilde{v}_\phi \rangle}_{\text{Reynolds stress}}, \quad (3)$$

where the first term is the convective flux and the second term is the toroidal Reynolds stress. The first term is usually neglected except for the regions where the fuelling is strong, for example, the ionization source region near the plasma edge, the core region in plasmas with NBI fuelling under low recycling conditions or in plasmas with central pellet injection. The second term is the toroidal Reynolds stress $\langle \tilde{v}_r \tilde{v}_\phi \rangle$ which can be written as

$$\langle \tilde{v}_r \tilde{v}_\phi \rangle = \underbrace{-\mu_\perp \nabla v_\phi}_{\text{diffusive term}} + \underbrace{V_{\text{pinch}} v_\phi + \Gamma_\phi^{RS}}_{\text{non-diffusive terms}}. \quad (4)$$

The first term, which is proportional to the velocity gradient, is a diffusive term, while the second and third terms are independent of the velocity gradient and are regarded as non-diffusive terms. The second term, which is proportional to the velocity itself, is called the momentum pinch, and changes its sign depending on the direction of rotation (co- or counter-rotation). In contrast, the third term is called the residual

stress, which does not explicitly depend on velocity shear or the velocity, and can be categorized as an off-diagonal term of the transport matrix [19]. This term can be expressed as proportional to pressure/temperature gradients, magnetic shear and poloidal velocity shear as a first order approximation. Note that the contribution from the radial electric field shear due to the toroidal rotation is categorized as a part of the diffusive term and leads to a 'renormalization' of this coefficient [20].

1.2. Magnetic field symmetry of tokamaks and helical plasmas

Historically, poloidal rotation in tokamaks and toroidal rotation in helical systems were neglected in the 1980s. This is because the poloidal flow is damped in tokamaks and toroidal flow in helical devices is damped due to parallel viscosity. In helical plasmas, the co-/counter-direction is defined such that the plasma current increases/decreases the rotational transform determined by external coil currents. Both the toroidal and poloidal flows were considered to be determined by the balance of the $j \times B$ torque of non-ambipolar fluxes and neoclassical viscosities. Because of the lack of toroidal symmetry and hence the large parallel viscosity in the toroidal direction, the toroidal flow is small and the radial diffusion of toroidal momentum can be neglected. However, it has now been recognized that the radial diffusion of toroidal momentum can be dominant in helical plasmas when the toroidal torque driven by tangential neutral beams becomes large.

In tokamaks, because of the toroidal symmetry of the system, the toroidal flow has been treated independently from the poloidal flow, and the toroidal flow was considered to be determined by the radial diffusion of toroidal momentum driven by the toroidal torque from neutral beams. However, when the toroidal magnetic field ripple amplitude is large, a neoclassical viscous effect in the toroidal direction is not negligible and the toroidal velocity agrees with the neoclassical prediction with ripple effects included [21]. The effect of neoclassical viscosity on toroidal flow is also recognized to be important when the toroidal symmetry is broken by the three-dimensional perturbed magnetic field.

1.3. Relation between perpendicular and parallel flow, and radial electric field

The radial electric field at the edge of H-mode plasmas is often dominated by a large poloidal rotation; the contribution of toroidal rotation to the radial electric field is small in most instances. However, in some cases (for example in the VH-mode [22, 23]), the toroidal rotation can have a significant contribution to the radial electric field and reduction of turbulent transport in the pedestal region. Since the suppression of turbulence causes a reduction of perpendicular viscosity and an increase in toroidal rotation velocity and $E \times B$ shear, toroidal rotation plays an important role in expanding the shear region more inside and making the pedestal region wider. There are different relative contributions to E_r from toroidal and poloidal velocities in H-mode, VH-mode and I-mode [24, 25]. The poloidal flow is dominated by the $E \times B$ drift and is determined by the pressure gradient, while the toroidal rotation is determined by momentum transport, which is discussed later.

There are significant differences in momentum, heat and particle transport. In general, the plasma pressure (both temperature and density) and density are constant on a magnetic flux surface, ψ, and they can be expressed as $p(\psi), n(\psi)$. However, the flow in the plasma, especially the poloidal flow, is not a magnetic flux function. In the case of axisymmetric plasmas, the toroidal angular speed, $\omega_\phi (= v_\phi/R)$, is approximately a magnetic flux function, but the poloidal angular speed, ω_θ, has a strong poloidal variation. The poloidal flow, which is usually a major contributor to the $E \times B$ flow (or perpendicular flow $v_\perp = (E \times B)/|B|^2 + (\mathrm{d}p_i/\mathrm{d}r)/(en_iZ_i)$), has a strong poloidal asymmetry due to the poloidal asymmetry of the radial electric field, E_r. Although the space potential, Φ, is constant on a magnetic flux surface, the radial electric field determined by the relation $E_r = (\mathrm{d}\Phi/\mathrm{d}\psi)(\mathrm{d}\psi/\mathrm{d}r)$ varies in the poloidal direction, except for the case of cylindrical low β plasmas. The radial electric field is decomposed as

$$E_r(\psi,\theta) = \frac{\nabla p_i(\psi)}{eZ_i n_i(\psi)} - (\omega_\theta(\psi,\theta)rB_\phi - \omega_\phi(\psi)RB_\theta). \quad (5)$$

Since the toroidal flow is not independent of the poloidal flow, because of the zero divergence of flow on a magnetic flux surface, the toroidal flow should have strong coupling to the radial electric field and poloidal flow.

When the local flow is discussed, the component of perpendicular flow, $v_\perp$, and parallel flow, $v_{||}$, are important because $v_\perp$ is determined by the radial profile of the potential and ion pressure, while $v_{||}$ is determined by the torque and parallel viscosity. In the case of axi-symmetric systems, the parallel viscosity in the toroidal direction (toroidal viscosity) vanishes because of the toroidal symmetry, and parallel viscosity only plays a role in the poloidal flow. (Of course this is not the case when the toroidal symmetry is broken in tokamak experiments.) Since the radial electric field is indispensable in reducing ripple losses in helical plasmas, the detailed structure of the radial electric field and poloidal flow has been intensively studied [26–32]. The mean poloidal flows are measured with charge exchange spectroscopy, while the fluctuating poloidal flows (zonal flows and GAMs) are measured with heavy ion beam probes in helical systems.

Strong poloidal variation of poloidal flow has been observed in the CHS heliotron where the measurement of poloidal rotation velocity over the whole plasma is available from charge exchange recombination spectroscopy [33]. In heliotron plasmas, the displacement of the magnetic axis is relatively large even in low β plasmas, as seen in the poloidal cross section (figure 2). The poloidal rotation velocity is larger on the outboard side ($R > 1.0\,\mathrm{m}$) where the magnetic flux surfaces are dense due to the shift of the magnetic axis. The poloidal asymmetry of the poloidal flow velocity observed in helical plasmas is due to the electrostatic potential being constant on magnetic flux surfaces. The poloidal asymmetry of the ion density can be explained by the conservation of the poloidal ion flux under strong toroidal viscosity.

In the momentum transport of toroidal flow, the toroidal flow angular speed $\omega_\phi = v_\phi/R$ is treated as a magnetic flux function and there is no explicit term of poloidal flow in the momentum transport equation (cross field diffusion equation is similar to heat and particle diffusion). However, since the toroidal rotation is determined by the radial force balance equation (equation (5)), the toroidal rotation is not independent
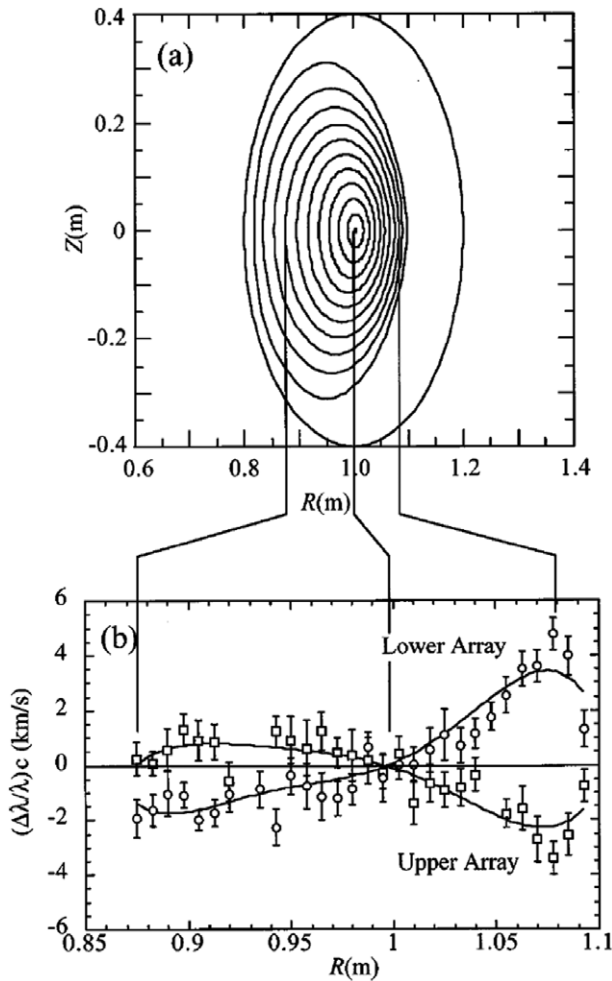
Figure 2. (*a*) Poloidal cross sections of magnetic flux surfaces and (*b*) the radial profile of the Doppler shift of the charge exchange line of C VI ($\Delta n = 8$–7, $\lambda = 529.05$ nm) in CHS. (From figure 1 in [33].) Reproduced with permission from Nishimura S. *et al* 2000 *Phys. Plasmas* **7** 437. Copyright 2000 AIP Publishing LLC.

of the poloidal rotation. There should be a link between the toroidal and poloidal flow since the magnetic field has poloidal and toroidal components. When the poloidal rotation velocity becomes large, an in-out asymmetry of toroidal angular speed is expected because of the flow compression due to the toroidal effect, a similar process to the Pfirsch–Schlüter current in the electron channel. In fact the ion 'Pfirsch–Schlüter flow', wherein the parallel flow is naturally produced in a toroidal plasma, was observed in the scrape-off layer with reciprocating Mach probes in JT-60U [34]. In the core plasma, a constant angular momentum speed is also experimentally confirmed in the DIII-D [35] tokamak, where the toroidal rotation velocity across the magnetic axis is available as seen in figure 3. The measured toroidal angular rotation speed profiles are consistent with the theoretical prediction that the angular rotation speed is only a function of the flux surface co-ordinate, and is independent of poloidal angle. However, it is not clear whether the assumption of the constant toroidal angular speed on a magnetic flux surface is valid near the plasma edge, where the ion 'Pfirsch–Schlüter flow' may play a role. Recently, the importance of toroidal flow near the LCFS has been recognized, because this momentum release from the region
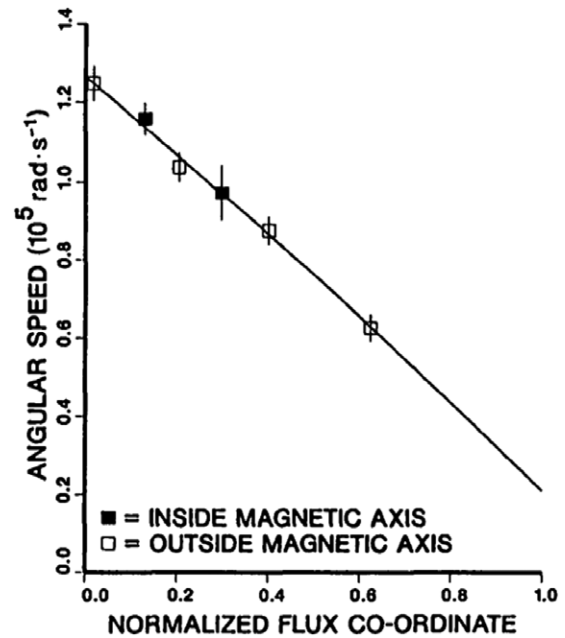
Figure 3. Angular rotation speed as a function of normalized flux co-ordinate measured with charge exchange recombination spectroscopy in DIII-D. (From figure 5 in [35].) Reproduced with permission from Burrell K. *et al* 1988 *Nucl. Fusion* **28** 3. Copyright 1988 IAEA Vienna.

inside the LCFS to the scrape-off layer is essential in driving spontaneous/intrinsic rotation.

2. Driving and damping

In tokamaks, the beam-driven term is often dominant, while both the non-ambipolar flux and the parallel viscosity are comparable to the beam-driven term. Recently the importance of the non-ambipolar flux and parallel viscosity has been recognized, especially in symmetry breaking experiments. There are several driving and damping forces in the plasma. In experiments it is not easy to distinguish whether the driving or damping forces play a role. For example, a decrease in the rotation velocity is not always due to an increase in damping forces. In many cases the decrease in rotation velocity is due to the appearance of a driving force in the opposite direction.

Toroidal torque driven by neutral beams is the most common in toroidal plasmas. The torque input from the beam can be calculated because the momentum transfer is through collisional processes, while the torque input from waves (RF and ECH) is difficult to calculate due to the complications of the mechanism. Therefore, most momentum transport studies (evaluation of the perpendicular viscosity, the so-called momentum diffusivity) have been carried out in plasmas with NBI. In this section, beam, RF and ECH driven-torques are discussed first.

2.1. Beam-driven torque

Tangential NBI is the most common method to provide toroidal torque in plasmas [36–48]. There are two mechanisms for momentum transfer from fast ions to the bulk: (i) quasi-instantaneous, or first orbit transfer, which results mainly from
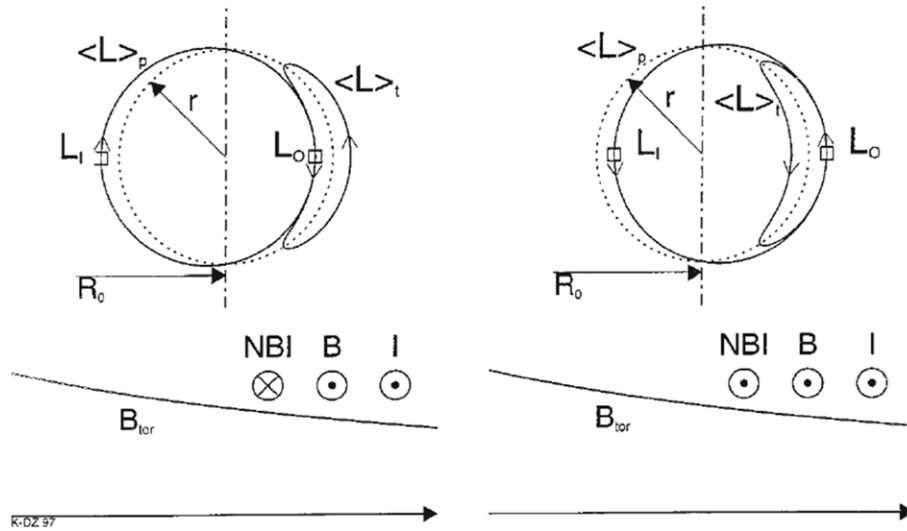
Figure 4. Drift surfaces for passing particles, absorbed inboard or outboard, and trapped particles for counter-injection (left) and co-injection (right). (From figure 4 in [49].) Reproduced with permission from Zastrow K.-D. *et al* 1998 *Nucl. Fusion* **38** 257. Copyright 1998 IAEA Vienna.

particles that are injected into trapped orbits, (ii) collisional transfer of momentum from passing ions to the bulk plasma during their slowing down process, which causes an enhancement of the total angular momentum of the rotating plasma. The toroidal torque is produced by the collision process between the bulk plasma and the fast ions. The calculation of the toroidal torque from neutral beams is relatively straightforward and the toroidal momentum diffusion coefficient has been evaluated in plasmas where toroidal torque from the neutral beams is dominant.

The ions have three constants of motion between collisions: kinetic energy, magnetic moment and the toroidal component of the canonical angular momentum. The toroidal angular momentum of each ion itself is not a constant of motion, although the toroidal angular momentum is conserved for the plasma as a whole. For ions injected parallel to the current in a tokamak plasma, the drift surfaces are shown in figure 4 [49]. The toroidal angular momentum averaged over the passing orbit, $\langle L \rangle_{\mathrm{p}}$, is larger than L_{I} at the point of absorption inboard and smaller than L_{O} at the point of absorption outboard as $L_{\mathrm{I}} < \langle L \rangle_{\mathrm{p}} < L_{\mathrm{O}}$. The toroidal angular momentum averaged over the trapped orbit, $\langle L \rangle_{\mathrm{t}}$, is much smaller than L_{O} ($\langle L \rangle_{\mathrm{t}} \ll L_{\mathrm{O}}$) and is given by the rate of precession of the banana orbit around the torus in the presence of the radial electric field that is set up by the rotating plasma.

Since the average minor radius over one drift surface is different from the minor radius at birth, and fast ions are continuously injected, there is a radial current of fast ions. The fast ion radial current is compensated for by an opposite current in the bulk plasma, resulting in a $J_r \times B_\theta$ force on the bulk plasma. An outward fast ion current produces a counter-current torque on the bulk plasma. Therefore, fast ion loss produces a torque in the counter-direction regardless of the direction of NBI (co-, counter- or perpendicular). The radial profile of perpendicular viscosity is almost identical to that of ion thermal diffusivity and the magnitude is similar in plasmas when the radial diffusion of the toroidal momentum driven by collisional momentum from tangentially injected neutral beams is dominant.
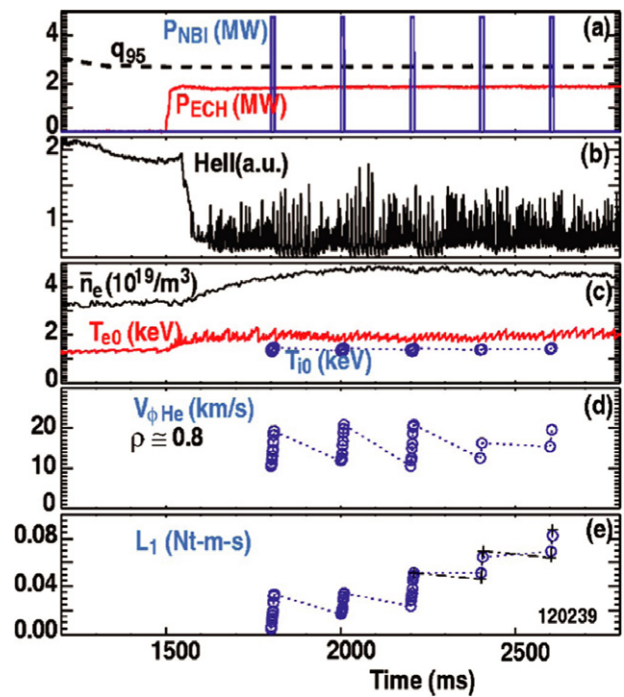
Figure 5. Time evolution of (*a*) safety factor, power of ECH and NBI, (*b*) He II light at divertor, (*c*) line-averaged electron density, and central electron and ion temperature, (*d*) toroidal rotation velocity of bulk He and (*e*) total integrated toroidal mechanical angular momentum, ratcheting up from NBI blip to blip in DIII-D. (From figure 3 in [50].) Reproduced with permission from deGrassie J.S. *et al* 2006 *Phys. Plasmas* **13** 112507. Copyright 2006 AIP Publishing LLC.

Toroidal flow driven by the $j \times B$ force of fast ions from beams is observed in experiments with NBI blips, where the pulse width is much shorter than the slowing down time scale [50]. Figure 5 shows the time evolution of the safety factor, power of ECH and NBI, He II light in the divertor, line-averaged electron density, central electron temperature

6
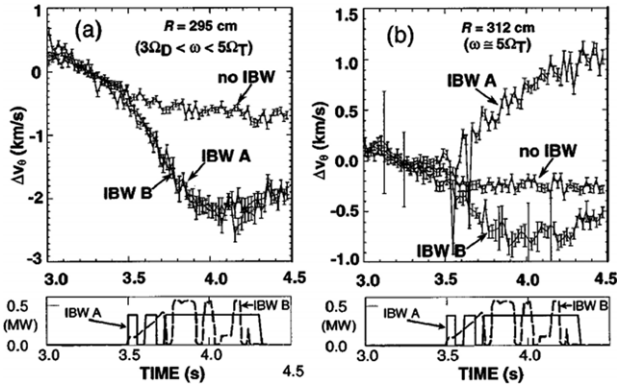
Figure 6. Time evolution of change in poloidal rotation velocity for IBW discharges with higher tritium density (IBW A) and lower tritium density (IBW B) and without IBW (no-IBW) at (*a*) $R = 295$ cm and (*b*) $R = 312$ cm in TFTR. (Figure 3 in [54].) Reproduced with permission from LeBlanc B.P. *et al* 1999 *Phys. Rev. Lett.* **82** 331. Copyright 1999 by the American Physical Society.

measured with electron cyclotron emission (ECE) and ion temperature, toroidal rotation velocity of bulk He and the total integrated toroidal mechanical angular momentum, L_ϕ, of the plasma calculated from the change in v_ϕ and the density profiles. Five NBI blips are applied to a steady-state ELMy H-mode discharge with constant NBI and ECH power. The NBI pulse width is 10 ms and much shorter than the volume averaged slowing down time and perpendicular scattering time of D^+ fast ions of 45 ms and 80 ms, respectively, because the collisionality of the plasma is relatively low (the electron density is 4×10^{19} m^{-3} and the electron temperature is 2 keV as seen in figure 5). Therefore, the change in toroidal rotation is due to the $J_r \times B_\theta$ force, and not due to the collisional transfer of momentum from passing ions during their slowing down process. It should be noted that there is only little relative change in T_i during the blips. Both the bulk ion (helium) and impurity (carbon) are accelerated, and the incremental velocities are compared with those predicted by the electric drift. The acceleration of toroidal flow due to the $J_r \times B_\theta$ force of fast ions is consistent with the dielectric constant having the neoclassical value.

### 2.2. RF-driven torque (MCFD, etc)

There are several observations of toroidal and poloidal flows driven by ICRF waves in tokamaks (see the overview paper [51]). Sheared poloidal flow has been observed in plasmas with ion Bernstein waves (IBWS) in TFTR and JET [52, 53]. Figure 6 illustrates rotation in IBW experiments from TFTR [54], where the temporal evolution of Δv_θ data from three discharges is overlain. Discharges labelled 'IBW A' and 'no-IBW' correspond to the two cases presented below. Discharge 'IBW B' had a significantly lower tritium density than IBW A. Looking at figure 6(*a*), it can be seen that between the $3\Omega_D$ and $5\Omega_T$ layers, at $R \approx 295$ cm, both IBW A and IBW B discharges have a similar behaviour, namely, that of a negative poloidal flow compared with the no-IBW case. On the other hand, IBW A and IBW B behave differently at $R \approx 312$ cm, near the $5\Omega_T$ layer. While IBW A shows a positive flow reaching 1 km s^{-1}, IBW B features a negative flow, falling to
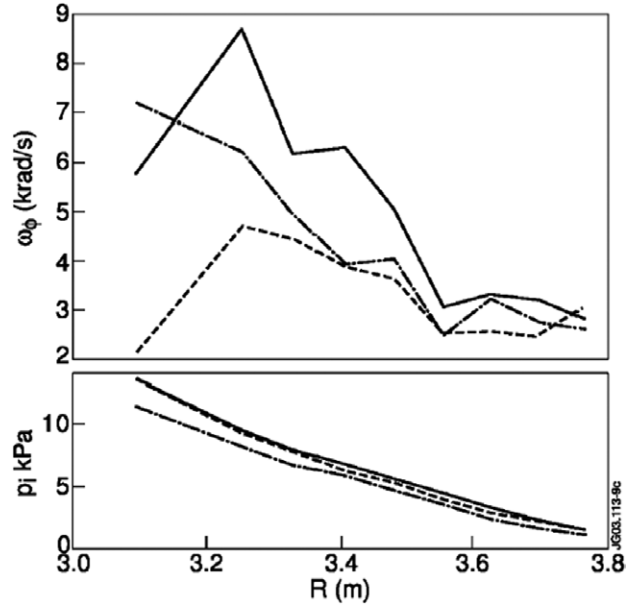
Figure 7. Radial profile of angular rotation speed and ion pressure for the discharge with $+90°$ (solid line) phasing and $-90°$ phasing (dashed line) ICRF and the discharge with LH (dotted–dashed line) in JET. (From figure 2 in [55].) Reproduced with permission from Eriksson L.-G. *et al* 2004 *Phys. Rev. Lett.* **92** 235001. Copyright 2004 by the American Physical Society.

-0.8 km s^{-1}. Shearing of the plasma poloidal rotation velocity was observed during application of IBWs. The observed sheared flow occurs near the tritium fifth harmonic cyclotron resonance layer and depends strongly on the tritium density, in agreement with the model. Furthermore, the model reproduces the observed insensitivity of the induced rotation to the tritium density in the region between the third deuterium harmonic layer and the fifth tritium harmonic layer.

Toroidal flow can arise when the fast ions resonating with ICRF waves are displaced radially and produce a radial current. This fast ion radial current is compensated for by an opposite current in the bulk plasma and results in a $J_r \times B_\theta$ force on the bulk plasma. In this process toroidal flow can be driven by RF waves through momentum transfer from the waves to the plasma via fast ions. There is no direct collisional momentum input in these experiments. In this case the driven flow is sensitive to the type of heating, such as mode conversion (MC) or minority heating (MH), rather than through the temperature or pressure gradient, which is a crucial parameter in the driving mechanism due to the residual stress discussed later. Changes of the toroidal plasma rotation induced by directed waves in the ICRFs have been identified experimentally [55]. The measured toroidal rotation and ion pressure profiles for three JET discharges are shown in figure 7 (note that the magnetic axis is at $R \sim 3$ m). The profiles show plasma rotation in the co-current direction. However, the discharge with $+90°$ phasing rotates significantly faster in the co-current direction over most of the radius than the $-90°$ discharge. Since $+90°$ phasing produces co-current propagating waves, this result is qualitatively consistent with an ICRF torque on the plasma. The rotation velocity for the reference discharge with LH heating lies in between the other two. The LH waves are directed, but carry only about 10% of
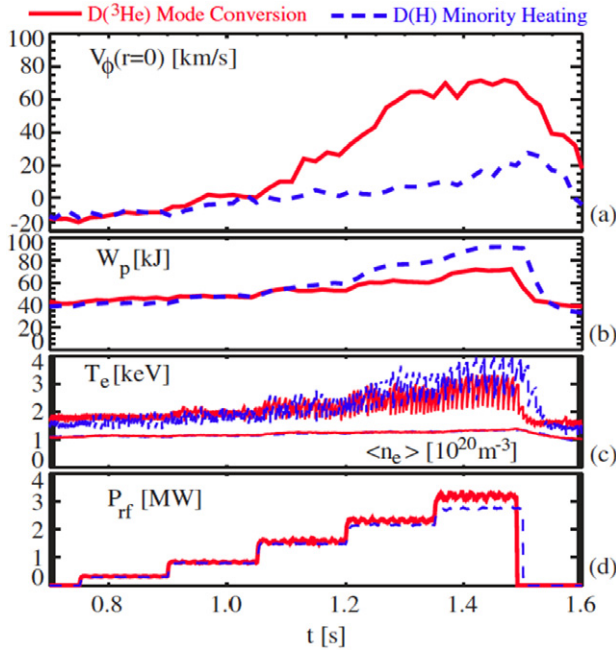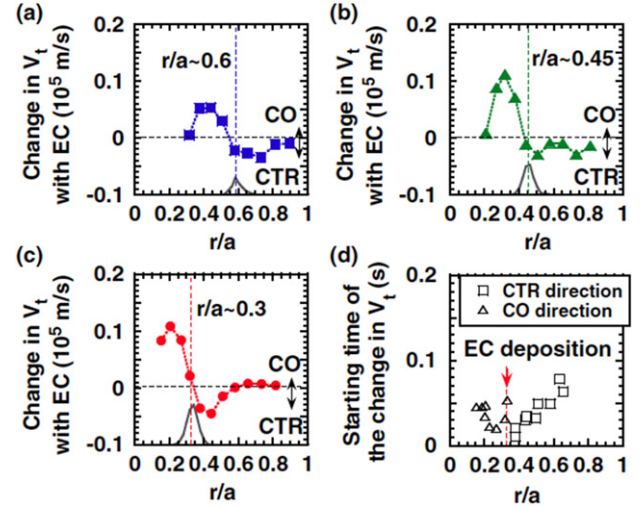
Figure 8. Time evolution of central toroidal rotation velocity, plasma stored energy, electron temperature, electron density and ICRF power with D(^{3}He) MC (solid lines) and D(H) MH (dashed lines) in Alcator C-Mod. (From figure 1 in [56].) Reproduced with permission from Lin Y. *et al* 2008 *Phys. Rev. Lett.* **101** 235002. Copyright 2008 by the American Physical Society.

Figure 9. Radial profile of change in toroidal rotation velocity for each EC deposition at (*a*) $r/a \sim 0.6$, (*b*) $r/a \sim 0.45$ and (*c*) $r/a \sim 0.3$ in the L-mode phase and (*d*) starting time of the change in toroidal rotation velocity towards the counter-direction (open squares) and co-direction (open triangles) in the case of (*c*) in JT-60U. (From figure 5 in [64].) Reproduced with permission from Yoshida M. *et al* 2009 *Phys. Rev. Lett.* **103** 065003. Copyright 2009 by the American Physical Society.

the momentum of the +90° ICRF waves for equal power. The ion pressure profiles for the +90° and −90° discharges are very similar, and the discharge with LH power has somewhat lower ion pressure. From these facts it can be concluded that the stronger rotation for +90° phasing is not due to a higher stored energy or stronger ion pressure. This experiment shows that the momentum carried by the ICRF waves is initially absorbed by fast resonating ions, which subsequently transfer it to the bulk plasma.

Strong toroidal and poloidal flows have been observed in D–^{3}He plasmas with ICRF MC heating on Alcator C-Mod [56–58] and JET [59]. The driven poloidal flow is localized near the MC layer, where strong damping of the mode converted ion-cyclotron wave is expected. A two-dimensional integral full-wave model is used to calculate poloidal forces driven by MC in tokamak plasmas [60]. The generation mechanism of plasma rotation by ion-cyclotron absorption of fast Alfvén waves is also proposed [61].

As seen in figure 8, the toroidal flow (rotation) velocity, derived from the Doppler shift of the x-ray spectra of Ar^{17+} impurities measured by high resolution x-ray spectroscopy, is significantly higher in the plasma with the MC ICRF than that in the plasma with MH ICRF. The toroidal flow driven by ICRF waves demonstrates that the momentum transfer process from the waves to the bulk plasma through the fast ion $J_r \times B_\theta$ force is occurring. This flow strongly depends on the heating scenario and the mode converted ion-cyclotron wave can drive the plasma with much higher efficiency than the case driven by MH. It is interesting that the radial current due to the fast ions is considered to be a non-ambipolar flux, which is one of the key elements of the driving mechanism in helical systems where there is no toroidal symmetry.

2.3. ECH-driven torque

When ECH is applied to the plasma, changes of toroidal rotation are commonly observed in tokamaks and helical plasmas. There are direct and indirect effects of ECH on toroidal rotation. The electrons coupled with ECH waves affect the radial electric field and poloidal rotation directly, while the increase in the electron temperature drives the enhancement of viscosity or the residual stress. Here the direct effect of ECH waves is discussed as an ECH-driven torque, and the indirect effects (due to the rise of the electron temperature) are regarded as changes in the Reynolds stress. As an example of the direct effect, trapped electrons coupled with ECH waves drive a non-ambipolar electron flux, a large positive electric field and poloidal rotation in helical plasmas [62], while the localized velocity shear appears near the electron cyclotron resonance (deposition layer) in tokamaks [63, 64].

Figures 9(*a*)–(*c*) show the changes in the measured toroidal rotation (V_t) in JT-60U plasmas with ECH for different EC deposition locations: $r/a \sim 0.6$, 0.45 and 0.3. The ECH power deposition profiles for each discharge are also plotted. The ECH power is 2.1 MW for the $r/a \sim 0.6$ deposition and 2.7 MW for the $r/a \sim 0.35$ and 0.45 depositions. It is clearly observed that the rotation inversion radius varies with the EC deposition radius. In the case with $r/a \sim 0.45$ and 0.3 depositions (figures 9(*b*) and (*c*)), ∇p_i becomes smaller with ECRH for $r/a < 0.5$. However, the time scale of the response of V_t is shorter than that of ∇p_i. In the $r/a \sim 0.3$ deposition case, a rapid change in V_t in the co-direction occurs first (∼0.02–0.04 s after EC injection), and then a slow change in co-rotation follows inside the EC deposition radius. On the other hand, ∇p_i in the core region ($r/a < 0.4$) gradually decreases and reaches a steady state at ∼0.07 s after the EC injection. From these results it can be concluded that ECH drives co-intrinsic rotation inside of the EC deposition
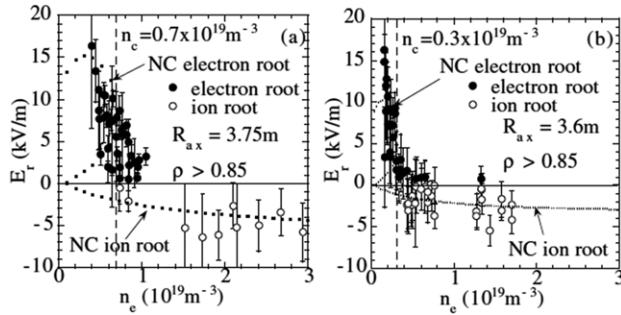
Figure 10. Density dependence of radial electric fields at $\rho > 0.85$ for plasmas with (*a*) standard configuration ($R_{ax} = 3.75$ m) and (*b*) inward shifted configuration ($R_{ax} = 3.6$ m). The dotted lines in (*a*) and (*b*) are neoclassical predictions in LHD. (From figure 1 in [67].) Reproduced with permission from Ida K. *et al* 2001 *Phys. Rev. Lett.* **86** 5297. Copyright 2001 by the American Physical Society.

radius and counter-intrinsic rotation outside. This experiment demonstrates that the ECH contributes to produce the velocity gradients, which is predicted by the residual stress, because the residual stress does not produce net toroidal rotation. This is in contrast to that where the residual stress produces net toroidal rotation at the H-mode pedestal by releasing the angular momentum from the boundary of the plasma to the scrape-off layer.

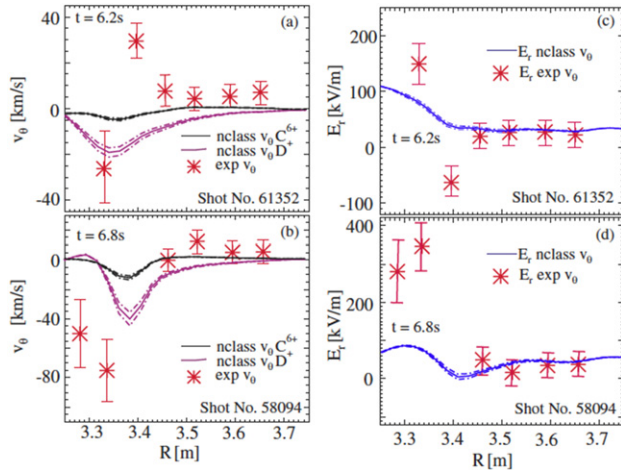### 2.4. Poloidal rotation and neoclassical predictions

For toroidal rotation, neoclassical effects can usually be neglected because turbulence dominates both in the damping and driving processes, although this could be important as a mechanism causing differences between the bulk and impurity rotation. In contrast, neoclassical effects can be large for poloidal rotation because the parallel viscosity overcomes the perpendicular viscosity. After the observation of large poloidal flow in H-mode plasmas, it has been an important issue whether the poloidal rotation is consistent with neoclassical predictions [65, 66]. The comparison of measured poloidal rotation with neoclassical predictions has been intensively studied in helical plasmas, where the poloidal rotation, and hence the radial electric field, is expected to suppress ripple losses. Ripple losses constitute a non-ambipolar flux, which can be suppressed by the radial electric field, and it produces a consistent radial electric field in the plasma. This is in contrast to fast ion loss in tokamaks, which is insensitive to the radial electric field because the energy of fast ions is much larger than the space potential in the plasma. Because the non-ambipolar flux due to ripple loss in plasmas with a radial electric field is much smaller than the ambipolar flux due to turbulence, it does not contribute much to the enhancement of transport in optimized stellarators. However, it contributes to the formation of the radial electric field, and hence poloidal and toroidal flow in the plasma.

Figure 10 shows a comparison of the measured radial electric field in LHD inferred from the poloidal rotation and that predicted by the neoclassical theory near the plasma periphery, $\rho > 0.85$, for two magnetic field configurations, with larger helical ripple ($R_{ax} = 3.75$ m) and smaller helical ripple ($R_{ax} = 3.6$ m) [67]. The radial electric field and

poloidal rotation are determined by the balance between the driving force due to ripple losses and the damping force due to the parallel viscosity. (In the neoclassical theory of helical plasmas, both forces are sensitive to the radial electric field and hence the balance equation between the ion and electron fluxes is used rather than the balance between the driving and damping force, with $\Gamma_i^{NC} = \Gamma_e^{NC}$ [68].) A clear transition from small negative electric field (called the ion root) to a large positive electric field (called the electron root) when the electron density (and collisionality, because the change in temperature is relatively small) decreases below a critical value (0.7×10^{19} m^{-3} for larger ripple and 0.3×10^{19} m^{-3} for smaller ripple). The absolute values of the radial electric field measured in the electron or ion root are the levels predicted by neoclassical theory. The critical electron density (and collisionality) required for transition from the electron root to the ion root is also in good agreement with the neoclassical prediction.

In the region of low collisionality below the critical density, there are three neoclassical solutions (the multiple solution regime): one is the electron root and the others are the ion and the intermediate root. Since the intermediate solution is unstable, it will not be realized in the plasma, and only two solutions are possible. The choice of either solution is determined by the continuity in the space and time domains. The measured values of the poloidal rotation velocity and radial electric field were found to be in qualitative agreement with those estimated by neoclassical theory. Note that the radial electric field outside the plasma boundary becomes positive regardless of collisionality because of the electron loss along the magnetic field [69]. This is in contrast to the toroidal rotation driven by the neutral beam torque, which is large enough to contribute to the radial electric field, because of toroidal symmetry in tokamaks. In helical systems the plasma flow tends to be parallel to the symmetry direction, in between the toroidal and poloidal directions. Experiments in helical plasmas show that the non-ambipolar flux accelerates the poloidal and toroidal flows with a combination such that the direction of the flow is nearly parallel to the symmetry direction.

It is an open question whether neoclassical theory is still valid in plasmas with transport barriers, where the scale lengths of the temperature or pressure gradient are comparable to the ion poloidal gyro-radius. The poloidal rotation measured in tokamaks sometimes agrees with that predicted by the neoclassical theory in the H-mode pedestal, but not in ITB regions [70]. Because of the large temperature gradient in the ITB region, the spin-up of poloidal rotation is expected. As seen in figure 11, the comparison of the measured poloidal rotation and radial electric field, and neoclassical predictions are investigated in JET plasmas. The poloidal rotation velocities of bulk ions (D$^+$) and impurities (C^{6+}), and the radial electric field are calculated using the neoclassical code NCLASS, based on the measured ion temperature and density profiles. Here positive poloidal rotation is in the electron diamagnetic direction. The poloidal rotation velocities measured are an order of magnitude higher than the neoclassical predictions for thermal particles in the ITB region. Therefore, the radial electric field evaluated from the measurements is much larger than that predicted by

Figure 11. Comparison of radial profiles of (*a*),(*b*) poloidal rotation velocity and (*c*),(*d*) radial electric field measured and predicted by neoclassical theory (NCLASS) for two discharges with ITBs in JET. (From figure 5 in [70].) Reproduced with permission from Crombé K. *et al* 2005 *Phys. Rev. Lett.* **95** 155003. Copyright 2005 by the American Physical Society.

neoclassical theory. It should be noted that the negative electric field in the middle of the large ITG region ($R = 3.4$ m) cannot be reproduced by the calculations.

Recently the bifurcation of poloidal rotation and the radial electric field has been observed in JT-60U H-mode plasmas [71]. There are two states in the magnitude of the radial electric field, one is in H-mode plasmas with small E_r and the other is in H-modes with large E_r, although the ion temperature and density gradients are unchanged. This observation suggests the existence of poloidal flow (radial electric field) driven by turbulence, because the neoclassical poloidal flow is proportional to the temperature gradient. Recent simultaneous measurements of both deuterium and carbon velocities in DIII-D show that differences between core deuteron and carbon rotation are inconsistent with the sign and magnitude of the neoclassical predictions in the intrinsic rotation H-mode conditions, and in plasmas with internal transport barriers (ITBs) [72].

2.5. Parallel viscosity due to magnetic field ripple

Parallel viscosity is the mechanism of flow damping due to collisions between passing and trapped particles in the local minimum of the magnetic field, such as those in banana orbits or helically trapped particles. In general the parallel viscosity plays an important role only in the poloidal direction, not in the toroidal direction, because of the toroidal symmetry in tokamaks. Therefore, only the parallel viscosity in the poloidal direction (poloidal viscosity) is important in tokamaks unless there is a perturbation in the magnetic field. (The case that the parallel viscosity in the toroidal direction becomes important is discussed below.)

Clear evidence of toroidal flow damping due to symmetry breaking of the magnetic field is a decrease in the toroidal rotation velocity due to an increase in toroidal ripple [73, 74]. These effects have been investigated experimentally in JET by changing the toroidal field (TF) ripple amplitude from 0.08% to 1% with the control of imbalance current between the two
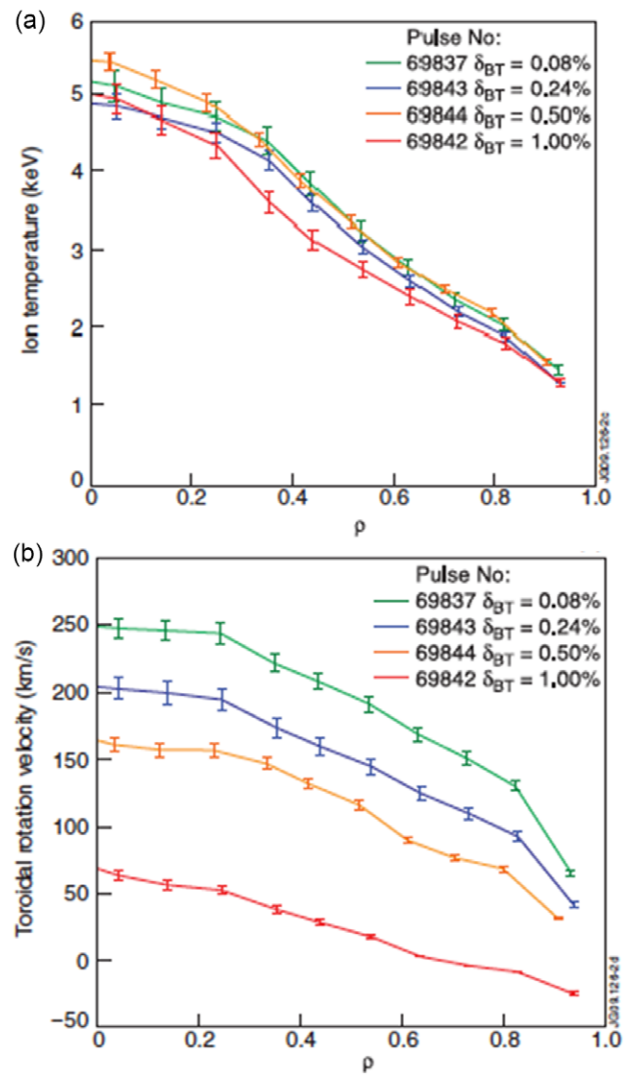
Figure 12. The ion temperature and toroidal rotation velocity profiles measured by CXRS in discharges with various toroidal magnetic field ripple in JET. (From figure 2 in [74].) Reproduced with permission from deVries P.C. *et al* 2010 *Plasma Phys. Control. Fusion* **52** 065004. Copyright 2010 IAEA Vienna.

coil sets (16 TF coils each, 32 TF coils in total). Similar experiments have been carried out in Tore Supra [75]. As seen in figure 12, the ion temperature profiles are almost unchanged during the scan of TF ripple. In contrast, the toroidal rotation velocity changes significantly, especially the edge rotation. In the regime of small TF ripple from 0.08% to 0.5%, the effect is only on the boundary condition (edge toroidal rotation velocity) and the gradient of toroidal rotation is almost unchanged. This is because the TF ripple does not penetrate very deeply inside the plasma. The effect of ripple is mainly localized at the plasma boundary in tokamaks. It is also interesting that the toroidal rotation is in the counter-direction when the TF ripple is 1%. This is from the toroidal torque due to the ripple loss of ions, which overcome the toroidal torque due to the neutral beam at the plasma boundary.

Similar results were obtained in JT-60U after the ferritic steel tiles (FSTs) were installed [76]. Before the installation of FSTs, the edge toroidal rotation was almost zero due to the TF
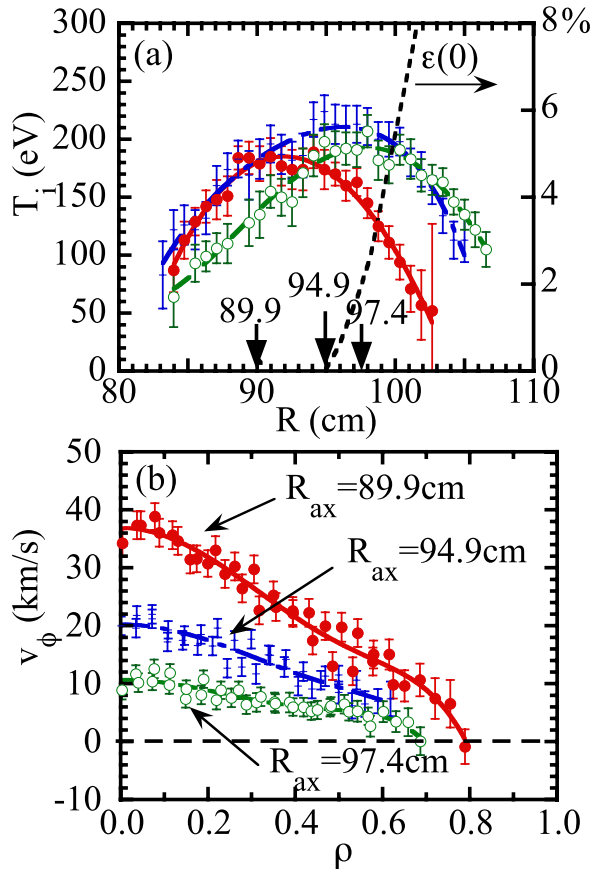
Figure 13. Radial profiles of ion temperature and toroidal rotation velocity in the plasma with different magnetic axis of $R_{ax} = 89.9$ cm (closed circles: small ripple), 94.9 cm (asterisks: medium ripple) and 97.5 cm (open circles: large ripple) in CHS. (From figure 1 in [77].) Reproduced with permission from Ida K. *et al* 1991 *Phys. Rev. Lett.* **67** 58. Copyright 1991 by the American Physical Society.

ripple (1%). After the reduction in the toroidal ripple by the FSTs, toroidal rotation near the plasma periphery ($\rho > 0.7$) significantly increased towards the direction of NBI for co-NBI discharges. In plasmas with perpendicular NBI, the magnitude of counter-rotation increased as the ripple loss power was increased in the peripheral region. This counter-rotation was reduced by installing FSTs as a consequence of the reduction in the ripple losses. The location of the driving source of counter-rotation agrees with the region where fast ion losses mainly take place.

In helical plasmas, the magnitude of the ripple is significantly larger than that in tokamaks, and it increases to 8% as seen in figure 13(*a*). The magnitude of the ripple at the magnetic axis in CHS depends on the position of the magnetic axis. In the configuration with an outward shift, the magnitude of the ripple at the magnetic axis can exceed 1% [77]. Figure 13 shows the radial profiles of ion temperature and toroidal rotation velocity for plasmas with small ($R_{ax} = 89.9$ cm), medium ($R_{ax} = 94.9$ cm) and large ripple ($R_{ax} = 97.5$ cm). The ion temperature slightly increases with the outward shift. In contrast, the toroidal rotation velocity drops by a factor of 4 by increasing the ripple. It is also noted that the decrease in the toroidal rotation gradient is observed even in the core region near the magnetic axis in helical plasmas, because the helical

ripple penetrates to the magnetic axis when the magnetic axis is shifted outward. This is in contrast to the effect of ripple in tokamaks which is mainly near the plasma edge.

In neoclassical theory, the toroidal viscosity is determined by the toroidal flow velocity, v_ϕ, the thermal velocity, $(2k_B T_i / m_i)^{1/2}$, (where k_B is the Boltzmann constant) and a geometric factor depending on the magnetic field (see [78]). The toroidal rotation velocity profile is dominated by perpendicular viscosity, which is comparable to the ion thermal diffusivity, in the configuration with inner axis shift, where the helical ripple is weak near the magnetic axis ($R_{ax} = 89.9$ cm). However, the parallel viscosity is found to be dominant in the configuration with an outer axis shift, where the ripple at the magnetic axis is large enough ($R_{ax} = 97.5$ cm). The toroidal viscosity measured in helical plasmas agrees with the parallel viscosity predicted by neoclassical theory.

### 2.6. Neoclassical toroidal viscosity

NTV has become highlighted after observations of the damping of toroidal flow due to magnetic braking in tokamaks [79–85]. Since there is no intrinsic toroidal viscosity, the NTV appears as a damping effect from magnetic braking, which is similar to the toroidal flow damping due to the parallel viscosity in helical systems. When there is large toroidal momentum input by tangential NBI, the toroidal flow is much larger than the poloidal flow. In these plasmas, a coupling term between the poloidal and toroidal flow has been neglected in the momentum transport equation. However, the damping of the poloidal rotation can drive toroidal flow, because of this coupling term. This is observed as an offset of toroidal flow driven by the poloidal damping force.

Figure 14 shows the toroidal and poloidal angular speed with and without magnetic braking by applying a resonant low $n/m = 1/1$ static error field in high confinement H-mode discharges in DIII-D [86]. Magnetic braking considerably decreases the toroidal rotation and thus reduces the core radial electric field and shear, which is expected to contribute to a reduction of turbulence in H-mode. In contrast, the effect of magnetic braking on the poloidal angular speed is relatively small. Since the contribution of toroidal rotation to the total radial electric field is dominant in this discharge, the radial electric field is reduced. It is a bit surprising that there is almost no change in the radial profiles of the electron density, and electron and ion temperatures, and thus particle and heat transport with and without magnetic braking, although the radial electric field shear is reduced by more than a factor of two in this experiment (except for the pedestal region in the plasma ($\rho > 0.9$)). This experiments suggests that $E \times B$ shear does not contribute to turbulence suppression at least in the plasma core region. The damping due to NTV is observed in tokamak plasmas with magnetic field perturbations which breaks the toroidal symmetry.

The existence of neoclassical toroidal rotation driven in the direction counter to the plasma current by non-axisymmetric, non-resonant magnetic fields has been confirmed in DIII-D experiments [87]. Evidence of an offset rotation in the direction counter to the plasma current caused by a non-resonant magnetic field is shown in figure 15, where a large amplitude static $n = 3$ field was applied to similar discharges with different rotation values. When the $n = 3$ field is
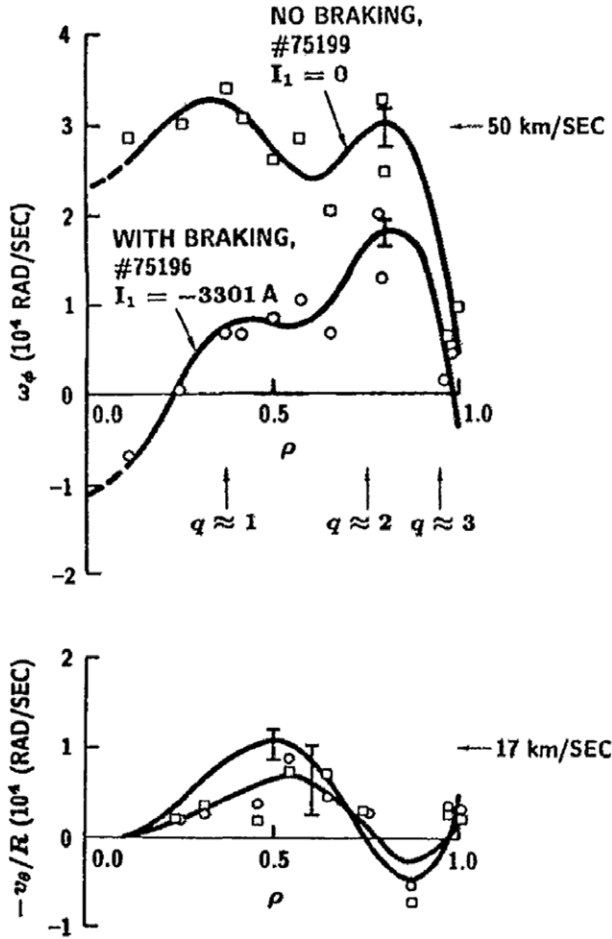
Figure 14. Radial profiles of toroidal and poloidal angular speed measured with He II and/or C VI ions, with and without magnetic braking in DIII-D. (From figure 5 in [86].) Reproduced with permission from LaHaye R.J. *et al* 1994 *Phys. Plasmas* **1** 373. Copyright 1994 AIP Publishing LLC.
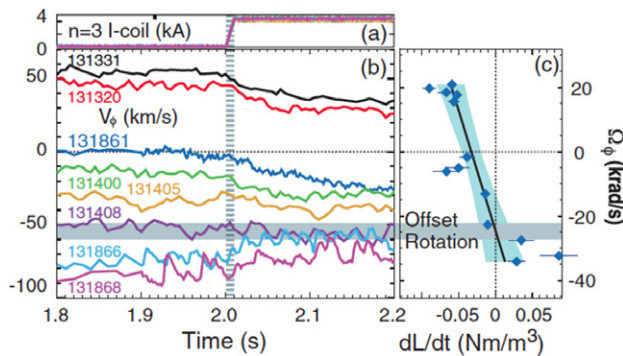
Figure 15. (*a*) Amplitude of $n = 3$ I coil current for plasmas with (*b*) different initial toroidal rotations. (*c*) Torque density (=dL/dt, where L is the angular momentum density) evaluated at $\rho = 0.8$ at the I coil current turn-on time for a larger number of discharges in DIII-D. (From figure 1 in [87].) Reproduced with permission from Garofalo A.M. *et al* 2008 *Phys. Rev. Lett.* **101** 195005. Copyright 2008 by the American Physical Society.

applied, a strong braking is observed for a co-rotating plasma and a smaller braking effect is observed for an already fast counter-rotating plasma, while a strong acceleration of the
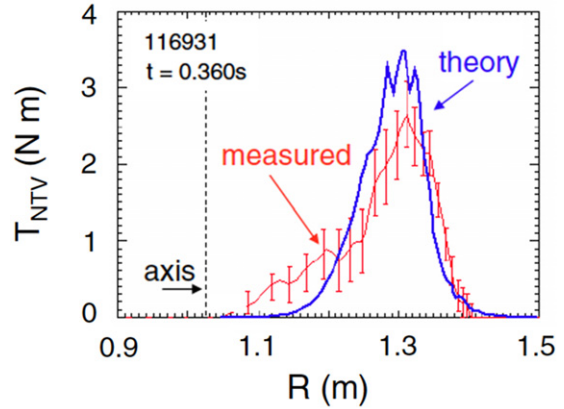
Figure 16. Comparison of measured d($I\Omega_\phi$)/dt profile to theoretical integrated NTV torque for an $n = 3$ applied field configuration in NSTX. (From figure 3 in [88].) Reproduced with permission from Zhu W. *et al* 2006 *Phys. Rev. Lett.* **96** 225002. Copyright 2006 by the American Physical Society.

plasma rotation in the counter-I_p direction is observed for near-stationary or slowly counter-rotating plasmas. The local torque applied by the $n = 3$ field has been measured at normalized minor radius $\rho \sim 0.8$ by calculating the change in the time derivative of the angular momentum density, L, at the time the $n = 3$ field is applied. The relation between the local torque densities measured and toroidal angular speed after the $n = 3$ is applied clearly demonstrates that the torque density is proportional to the velocity difference from the offset rotation as dL/d$t \propto (v_\phi - v_\phi^{\text{offset}})$, where the v_ϕ^{offset} is an offset rotation due to the NTV caused by the magnetic braking using the $n = 3$ perturbation magnetic field. The observed magnitude, direction and radial profile of the offset rotation are consistent with neoclassical theory predictions.

A quantitative comparison of neoclassical viscosity was carried out in the NSTX tokamak [88]. The change in the measured plasma angular momentum profile is compared with the theoretical NTV torque by evaluating the angular equation of motion dΩ_ϕ/d$t = T_j$, where the torques T_j are due to (i) NTV, T_{NTV}, (ii) momentum input from high-power co-injected neutral beams, T_{NBI}, (iii) electromagnetic forces on rotating magnetic islands (resistive MHD modes), $T_{J \times B}$, and (iv) fluid viscous forces between adjacent flux surfaces, $T_{\mu\perp} [\propto \mu_\perp \nabla v_\phi]$. $T_{\mu\perp}$ can be calculated from $\mu_\perp$, which is evaluated from a similar discharge. The damping due to $T_{J \times B}$ is initially localized near the island, and diffuses from this radius, leading to a local flattening of and a distinctive momentum diffusion across the rational surface. In contrast the damping due to T_{NTV} is relatively rapid, global, and the rotation profile decays more or less simultaneously in the wide region of the plasma.

In this experiment the NTV is dominant and much larger than the torque due to perpendicular viscosity ($T_{\mu\perp} < 0.15 T_{\text{NTV}}^{\text{peak}}$) and the change in beam-driven torque ($\Delta T_{\text{NBI}} \sim 0.02 T_{\text{NTV}}^{\text{peak}}$). The radial profile of the measured NTV, T_{NTV}, shows good agreement with that predicted by the theoretical calculation as seen in figure 16. The NTV has a peak at $R = 1.3$ ($\rho = 0.6$) with a magnitude of ~ 3 N m. The magnitude, evaluated from the damping rate of the toroidal flow, is consistent with the NTV model. Quantitative agreement between experiment and theory is found when the effect of

toroidally trapped particles is included. In symmetry breaking experiments, the offset rotation is also observed and the magnitude, direction and radial profile of the offset rotation are consistent with neoclassical theory predictions.

There are several mechanisms in determining the magnitude of NTV, because of the plasma response to the magnetic field perturbation, such as plasma resonant field amplification (RFA) and Lagrangian effects [89]. Therefore, a precise comparison between the NTV torque experimentally determined and calculated with the NTV model needs further development [90].

Finally, there are a few miscellaneous rotation damping mechanisms, such the effect of ELMs [91] and neutrals [92].

3. Reynolds and kinetic stresses

As discussed above, the Reynolds stress consists of diffusive and ND terms. The diffusive term is the stress which is proportional to the velocity gradient and therefore vanishes when there are no velocity gradients. There are two important ND terms; one is the pinch, which is proportional to the velocity and the other is the residual stress, which does not depend on the velocity and its gradient. Since the residual stress is driven by turbulence and depends on the temperature gradient, it is regarded as an off-diagonal term of the transport matrix. The pinch term, driven by the thermodynamic force [93, 94], is also regarded as an off-diagonal term in the transport matrix, because this term depends on the temperature gradient as well. Because of the existence of the residual stress, the plasma can rotate without external torque, as discussed in section 2; this rotation is called intrinsic/spontaneous rotation and the divergence of the stress is equivalent to an intrinsic torque. There have been many observations of intrinsic rotation [95]. Historically it is well known that there is significant toroidal rotation even in ohmic L-mode plasmas where there is no external toroidal torque [96–103], in some cases consistent with neoclassical predictions and in others clearly turbulence driven. Intrinsic toroidal rotation has been also observed in plasmas with ICRF [104–109] and LHCD [110–116]. Intrinsic rotation becomes more significant in plasmas with edge transport barriers such as H-mode and I-mode [117–132], and with ITBs [133–135].

3.1. Diffusive term

When there is a toroidal flow velocity gradient in the radial direction, the perpendicular viscosity in the region of velocity shear contributes to the transfer of toroidal momentum. The viscosity coefficient is expressed as $\mu_\perp$ or χ_ϕ from the analogy with the ion thermal diffusivity χ_i. It is well known that the diffusive term of momentum transport is turbulence driven, and early experiments showed this viscosity coefficient has a magnitude similar to the ion thermal diffusivity as $\mu_\perp \sim \chi_i$. The ratio of ion thermal diffusivity to the perpendicular viscosity coefficient is called the Prandtl number, P_r, and an interesting question arises concerning the value of this number in turbulence-dominated plasmas. Since there are ND terms in momentum transport, the precise evaluation of the viscosity coefficient is not easy. If the intrinsic flow due to the ND term is neglected, the viscosity coefficient and momentum
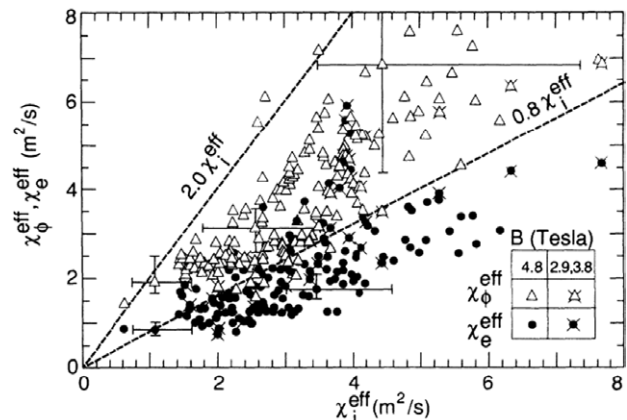

Figure 17. Measured effective thermal and momentum diffusivities for all discharges in the experiment in the region $0.3 \leqslant r/a \leqslant 0.8$ in TFTR. (From figure 3 in [141].) Reproduced with permission from Scott S.D. *et al* 1990 *Phys. Rev. Lett.* **64** 531. Copyright 1990 by the American Physical Society.

confinement time as global parameters can be over or under estimated, depending on the direction of the intrinsic plasma flow (co-direction or counter-direction).

Although both the diffusive and ND terms should be evaluated in order to calculate the Prandtl number, it is not possible to distinguish diffusive and ND terms of momentum transport in steady-state plasmas. As such, the viscosity coefficient and momentum confinement time are evaluated as 'effective' viscosity and Prandtl number by ignoring ND terms. There have been many experiments for the evaluation of the Prandtl number in various tokamaks (DIII-D [136], ASDEX [137], JET [138–140], TFTR [141]), because of the importance in understanding the mechanism of turbulent transport in toroidal plasmas.

Simultaneous profile measurements of the toroidal rotation speed and ion temperature during unbalanced NBI show that the perpendicular viscosity and thermal diffusivities are comparable in magnitude ($\mu_\perp = 1.5\chi_i$) and vary similarly with plasma current and minor radius in TFTR [141], as seen in figure 17. In this experiment the electron thermal diffusivity is smaller than the ion thermal diffusivity ($\chi_e = 0.5\chi_i$). There is considerable theoretical interest in such correlations. The ITG-driven class of instabilities (ITG modes) is predicted to have equal levels of ion heat and momentum diffusivity ($\mu_\perp \approx \chi_i$), and collisionless trapped electron modes (CTEMs) are predicted to have equal levels of ion and electron heat diffussivities ($\mu_\perp \approx \chi_i \approx \chi_e$). The correlation of $\mu_\perp$ and χ_i is consistent with anomalous transport driven by collisionless electrostatic micro-instabilities including ITG modes and CTEMs. In this experiment there was a high toroidal rotation velocity ($\sim$500 km s^{-1}) driven by tangential NBI, and offset rotation due to NTV and spontaneous/intrinsic rotation, which will be discussed later in this paper, are masked by the large rotation driven by NBI.

The results from TFTR differ somewhat from the results in JET, where the perpendicular viscosity is significantly smaller than the ion thermal diffusivity [142]). Generally the Prandtl number was found to be significantly below unity, $0.18 < P_r < 0.35$ in JET, although it is predicted that momentum and heat diffusivity are equal in ITG-dominated
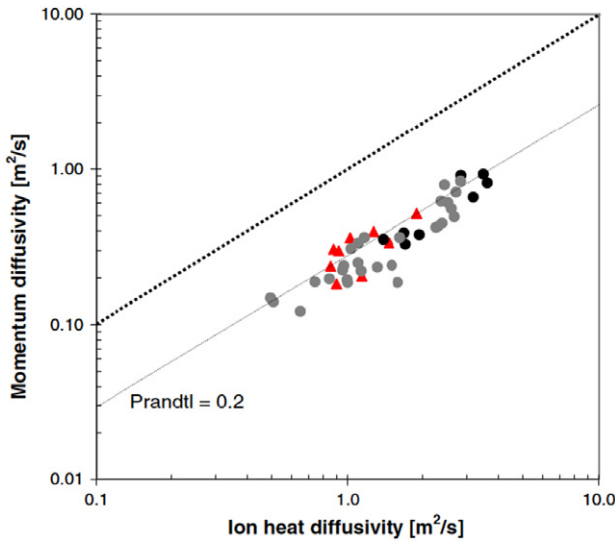
Figure 18. The momentum diffusivity as a function of the ion heat diffusivity averaged over the gradient region ($0.3 < \rho < 0.7$). The high density ELMy H-mode discharges are shown as red triangles. Other H-mode discharges are included, shown as black and grey dots. The error on both diffusivities is of the order of 15% in JET. (From figure 8 in [142].) Reproduced with permission from deVries P.C. *et al* 2006 *Plasma Phys. Control. Fusion* **48** 1693. Copyright 2006 IAEA Vienna.

plasmas (see figure 18). Comparison of the confinement times of angular momentum and energy reveals close similarities between thermal and perpendicular momentum transport. The ratio of momentum to energy confinement time, τ_ϕ/τ_E, is close to unity in L-mode; however, the ratio is significantly larger ~ 2 in plasmas with counter-NBI.

It should be noted that the ND term of momentum transport described later is ignored in the transport analysis in these studies. Therefore, when spontaneous/intrinsic co-rotation exists in discharges with co-NBI, the viscosity coefficient and the Prandtl number will be underestimated. For momentum transport it is important to evaluate the viscosity coefficient both for co-rotation and counter-rotation because the ND term causes a disparity between co- and counter-NBI plasmas, which will be discussed later. The apparent differences in perpendicular viscosity and momentum confinement time between co-NBI and counter-NBI have been experimentally observed in ASDEX [143]. The difference was phenomenologically understood to be different confinement. However, the physics behind causing the difference in viscosity coefficient between co- and counter-NBI is unclear, because the plasma rotation itself should have no impact on turbulence, although rotation shear can contribute to turbulence suppression.

As seen in figure 19, the radial profile of toroidal angular speed is significantly peaked in the discharge with counter-NBI compared with that with co-NBI. The perpendicular viscosity coefficient (indicated as momentum diffusivity χ_ϕ in [143]) with counter-NBI is much smaller than that in the co-NBI plasma, by a factor of 5 or more. This is in contrast to the reduction of viscosity due to the transition from L-mode to H-mode, which is only by a factor of two or less. Although there are significant apparent differences in magnitude of the perpendicular viscosity, the ion confinement is almost identical
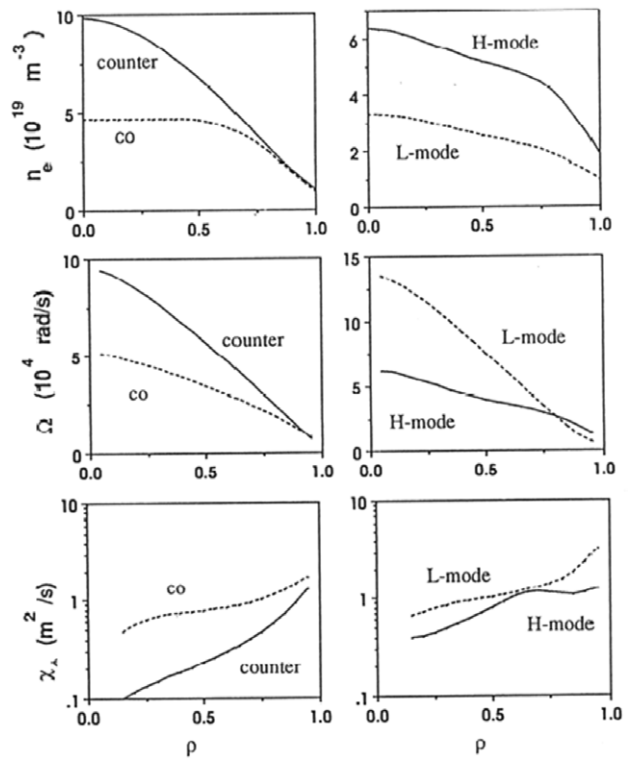

Figure 19. Radial profiles of electron density, absolute value of toroidal angular speed, viscosity (momentum diffusivity) in discharges with co- and counter-NBI, and L-mode and H-mode plasmas. Note that the sign of the toroidal angular speed is different between these two discharges. It is positive in the discharge with co-NBI and negative in the discharge with counter-NBI. (From figure 7 in [143].) Reproduced with permission from Kallenbach A. *et al* 1991 *Plasma Phys. Control. Fusion* **33** 595. Copyright 1991 IAEA Vienna.

between co-NBI and counter-NBI plasmas. The momentum diffusivity is much smaller than the ion thermal diffusivity in the counter-NBI discharge, while it is comparable in the co-NBI discharge.

Similar results were obtained in the parallel and perpendicular-NBI experiment in PBX [144]. Although the ion confinement does not depend on the configuration of NBI (2 para-NBIs, 1perp-NBI + 1 para-NBI, 2 perp-NBIs), the global momentum confinement time strongly depends on the NBI combination. The momentum confinement time for the plasma with two perpendicular NBIs was 147 ms and much larger than that of the plasma with two parallel NBIs (35 ms). The significant increase in momentum confinement time may be due to the contribution of spontaneous/intrinsic rotation, and may not be due to the reduction in viscosity, because the ion thermal diffusivity is almost unchanged.

3.2. Pinch term

The momentum pinch has been discussed as one of the candidate ND terms in momentum transport. Early momentum pinch models [145] have been developed by more sophisticated treatments. The theoretical underpinning of this term is the TEP pinch which is also called the Coriolis pinch [146]. This term causes a peaking of toroidal rotation regardless of the rotation direction, and determines the velocity profile shape.
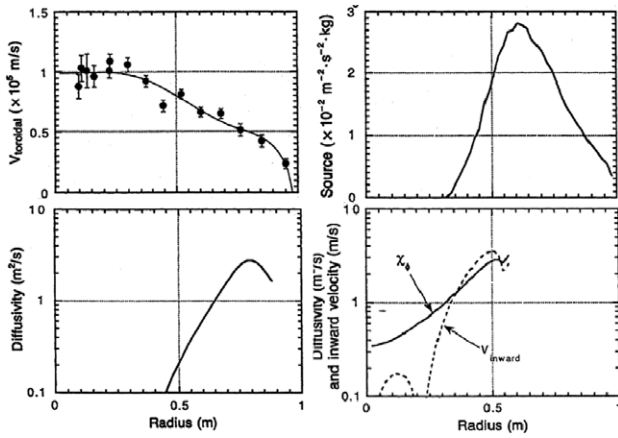
Figure 20. Radial profiles of measured toroidal velocity, momentum source and momentum diffusivity in steady-state momentum balance analysis and momentum diffusivity (solid line) and V_{inward} (dashed line) obtained from modulation analysis for off-axis beam injection in JT-60U. (From figure 3 and 6 in [159].) Reproduced with permission from Nagashima K. *et al* 1994 *Nucl. Fusion* **34** 449. Copyright 1994 IAEA Vienna.

This is one of the toroidal effects which can be visible in low aspect ratio devices, where the moment of inertia density in a toroidal shell in the core is smaller than that in the edge. In this case, when the momentum is homogenized by turbulence, it causes a pinch of angular momentum and the core rotates faster. Here the mechanism which is linked to the relation between angular momentum and linear toroidal momentum, P_ϕ, is also important. The concept of the pinch is the mechanism invoked to explain the peakedness of the rotation profiles observed in certain experiments not explained directly by spontaneous rotation itself. Even though there is no toroidal torque, toroidal velocity profiles of ELM-free H-mode plasmas are centrally peaked, which suggests the presence of an inward momentum pinch, as reported in Alcator C-Mod [147, 148].

It is a crucial issue in future tokamaks such as ITER whether the small toroidal rotation with low torque input is large enough to stabilize the RWM. The threshold toroidal rotation to stabilize the RWM has been investigated in experiments. The minimum toroidal rotation required to stabilize the RWM with the no-wall stability limit was found to be less than 1% of the Alfvén velocity in DIII-D [149], while it is more than 5% for plasmas with $q = 2$ in NSTX [150]. This would be due to the fact that the critical toroidal rotation is sensitive to plasma parameters. Since there is a large uncertainty in the toroidal rotation velocity required for the stabilization of RWMs, the operational scenario which realizes large toroidal rotation with enough margin is necessary. Therefore, a physics understanding of intrinsic rotation and the momentum pinch has become a highlighted issue, and there have been many experiments on the momentum pinch in DIII-D [151], JET [152–155] and NSTX [156], JT-60U [157, 158].

Peaked toroidal rotation profiles were observed in plasmas with off-axis tangential NBI in JT-60U [159], which suggests the existence of a momentum pinch. Figure 20 shows the radial profiles of toroidal rotation velocity and momentum source (toroidal torque) with off-axis injection. Although there is no momentum source near the magnetic axis with $\rho < 0.3$, there is a finite gradient of toroidal rotation

velocity observed. In the steady-state momentum transport analysis with only the diffusive term, the viscosity coefficient (momentum diffusivity χ_ϕ) decreases sharply towards the magnetic axis because of the lack of a momentum source near the plasma centre. The magnitude of the viscosity coefficient drops below $0.1\,\text{m}^2\,\text{s}^{-1}$, which is much smaller than the ion thermal diffusivity. By modulating the NBI, diffusive and ND terms can be evaluated from the radial profile of phase delay and amplitude. In this experiment the ND term is assumed to be proportional to the toroidal rotation velocity, v_ϕ, as a pinch term $V_{\text{inward}}v_\phi$. With the diffusive-pinch model, the viscosity coefficient (momentum diffusivity) χ_ϕ decreases gradually towards the plasma centre and reaches $0.4\,\text{m}^2\,\text{s}^{-1}$, which is comparable to the level of ion thermal diffusivity. The values are only shown in the region of $r < 0.6\,\text{m}$, because of the limitations imposed by experimental errors. In this experiment the relation between the ND term, $\langle \tilde{v}_r \tilde{v}_\phi \rangle^{\text{ND}}$, and toroidal rotation, v_ϕ, has not been checked experimentally. (Therefore, the $\langle \tilde{v}_r \tilde{v}_\phi \rangle^{\text{ND}} \propto v_\phi$ is not an experimental result, but an assumption.)

Recently a similar approach (NBI modulation) has been taken in order to investigate the ND term of momentum transport. The essential ingredient in the study of pinch terms is an off-axis momentum source. This is analogous to particle transport where the concept of the particle pinch is adapted in order to explain the peaked density profile with edge fuelling. It is therefore interesting to measure the toroidal rotation profiles in the plasma where the momentum source is localized near the plasma edge. Since tangential beams are arranged to impart toroidal momentum to the plasma core, the toroidal torque input from the injected particles to trapped orbits or collisional transfer of momentum from passing to bulk ions is inefficient near the plasma edge. On the other hand, the $j \times B$ torque by perpendicular NBI should be an efficient tool to produce toroidal momentum near the plasma edge.

The radial profiles of phase delay and amplitude were measured in JT-60U using the modulated perpendicular neutral beam in order to evaluate the diffusive and ND terms [160]. The monotonic phase delay in figure 21(*b*) indicates that the momentum source is localized near the plasma edge with $\rho \sim 0.8$. The amplitude increases during the propagation in the region of $0.4 < r/a < 0.6$, which corresponds to the rapid decrease in inward velocity ($\mathrm{d}V_{\text{pinch}}/\mathrm{d}r < 0$). The radial profiles of the viscosity coefficient (momentum diffusivity) and pinch velocity (convective velocity) are derived from the phase delay and amplitude. The steady-state toroidal rotation profile in L-mode plasmas with counter-NBI can be reproduced using the viscosity coefficient and pinch velocity given by the modulation experiment. However, the steady-state profiles in L-mode and H-mode plasmas with co-NBI cannot be reproduced by these coefficients. The discrepancy is attributed to the spontaneous/intrinsic rotation due to the ion pressure gradient, which is equivalent to the residual stress-driven rotation discussed later.

A physical model of the TEP of plasma angular momentum has been developed in [161]. There are two mechanisms which contribute to the pinch term of toroidal momentum transport. One is the TEP pinch velocity driven by the magnetic field curvature $\propto 1/R$. The magnitude of the pinch depends on the localization of turbulence in the bad
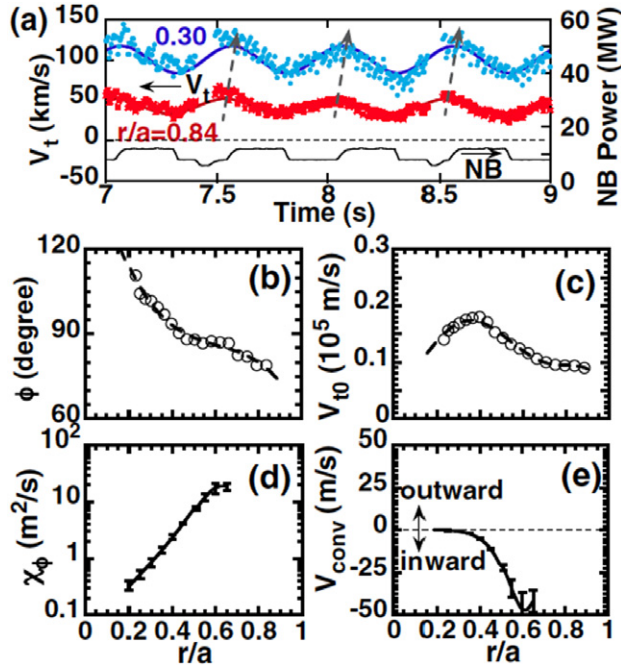
Figure 21. (*a*) Time evolution of V_t response to the modulated beams at $r/a = 0.84$ and 0.30, and waveform of NB power in the H-mode discharge. Radial profiles: (*b*) phase delay (*c*), modulation amplitude, (*d*) viscosity coefficient (momentum diffusivity), (*e*) pinch velocity in JT-60U. (From figure 2 in [160].) Reproduced with permission from Yoshida M. *et al* 2008 *Phys. Rev. Lett.* **100** 105002. Copyright 2008 by the American Physical Society.
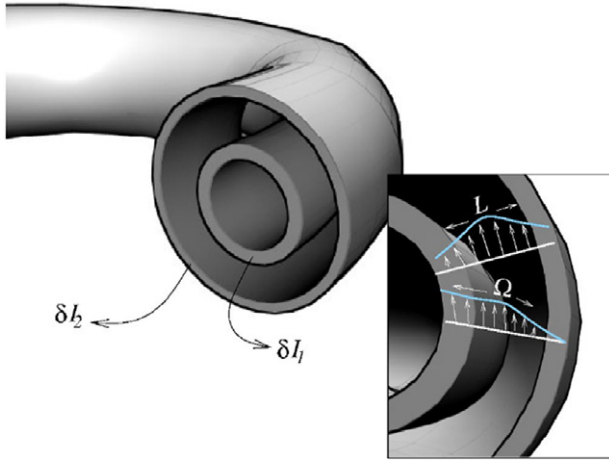
Figure 22. Two toroidal shells of moment of inertia densities δI_1 and δI_2. Since $\delta I_1 < \delta I_2$, the core has less moment of inertia density than the edge; as a result, when the momentum is homogenized, the core rotates faster. (From figure 1 in [161].) Reproduced with permission from Gürcan O.D. *et al* 2008 *Phys. Rev. Lett.* **100** 135001. Copyright 2008 by the American Physical Society.

curvature region. In the case of turbulence with ballooning structure, it scales as the inverse of major radius ($1/R$). The second mechanism is linked to the relation between angular momentum and linear toroidal momentum. Due to the conservation of angular momentum, the toroidal rotation can be accelerated when the inertia density decreases towards the magnetic axis. This is illustrated in figure 22. Because of the

toroidal effect (geometric effect), the core has less moment of inertia density than the edge; as a result, when the momentum is homogenized, the core rotates faster. This is the acceleration of toroidal speed which appears in the process of conversion from angular momentum to linear momentum, and scales as ϵ_0/R ($\epsilon_0 = a/R_0$ where a is minor radius and R_0 is the major radius of the magnetic axis).

By taking account of these two mechanisms, the pinch velocity for the momentum can be expressed as [161]

$$V_{\mathrm{pinch}} = 2\mu_\perp[-(F + \epsilon_0(r/a))/R] \tag{6}$$

and

$$F \equiv \langle |\tilde{v}_r|^2 (\cos\theta + \hat{s}\sin\theta)\rangle / \langle |\tilde{v}_r|^2 \rangle, \tag{7}$$

where F is the poloidal asymmetry of turbulence magnitude. $F = 0$ for poloidally symmetric flute-like turbulence intensity and $F \simeq 1$ for strongly outward (low magnetic field side) localized ballooning.

This model has two important aspects for the characteristics of the pinch term. One is poloidally asymmetric ballooning type turbulence localized outwards associated with magnetic field curvature, and the other is a change in inertia density due to toroidal effects. These effects can be strong in high β plasmas of low aspect ratio tokamaks, especially spherical torii, but should be weak in low β and low aspect ratio tokamaks, and helical plasmas where ballooning type fluctuations do not play an important role because of the helical structure of the weak magnetic field side. (It should be noted that the ND term of momentum transport is as significant as in tokamaks.)

The other theoretical model for the pinch term is the Coriolis drift. The pinch velocity due to the Coriolis drift effect based on gyro-kinetic calculations has a formula similar to the TEP but gives larger values, which is expressed as [162]

$$V_{\mathrm{pinch}} = \mu_\perp[-4/R - L_n^{-1}], \tag{8}$$

where $L_n^{-1} = \nabla n/n$ is the inverse scale length of the density profile. The second term is another inward pinch term due to the density gradient. This term is small if the density profile is flat (e.g. as in the core in H-mode), but near the edge where the density gradient is large, the second term may dominate. If one takes the large aspect ratio limit, and chooses $F = 1$, there is a factor of 2 difference between the two expressions for the plasma with a flat density profile. This comes from the different assumptions in these two works (rigid rotation is assumed in the Coriolis drift model but not in the TEP model).

A broad survey of the experimental database of neutral beam heated plasmas has been carried out in the JET tokamak [163]. Figure 23 shows the radial profiles of the pinch and Prandtl number at various radii. The Prandtl number is close to unity, which is much larger than the results shown in figure 18. This is due to the contribution of the ND terms in the momentum transport analysis. When the ND term is neglected, the viscosity coefficient and Prandtl number are significantly underestimated because the ND term is comparable to the diffusive term in these experiments. The measured pinch and Prandtl number are consistent with those predicted by GKW simulations, which depends on an assumption of wave numbers. These results may suggest
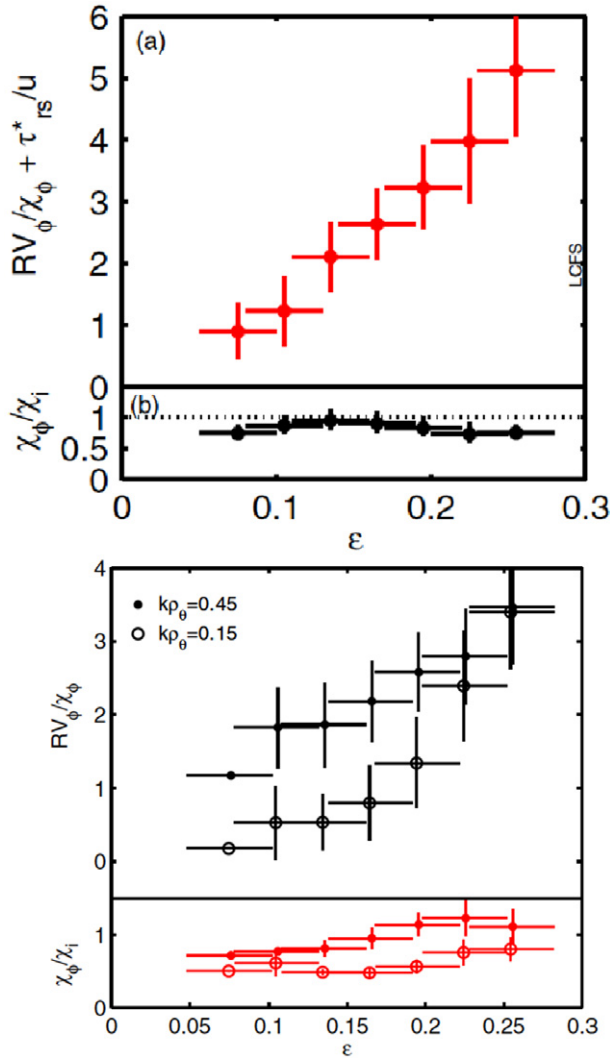
Figure 23. Profiles of (*a*) average and standard deviation of pinch number and Prandtl number for seven radial intervals in (*a*) experiment and (*b*) GKW calculation for two different wave numbers in JET. (From figures 2 and 4 [163].) Reproduced with permission from Weisen H. *et al* 2012 *Nucl. Fusion* **52** 042001. Copyright 2012 IAEA Vienna.

the existence of a convective transport mechanism which has its origin in the vertical particle drift resulting from the Coriolis force. However, in order to test whether the ND term observed is due to the pinch term of the Coriolis drift or not, it is important to have a similar comparison in discharges with counter-NBI (anti-parallel to the plasma current). This is because if the ND term is due to the residual stress (which contributes to spontaneous/intrinsic rotation in the co-direction), the viscosity coefficient and Prandtl number will be underestimated for co-rotating plasmas but be overestimated for counter-rotating plasmas. In the case of a pinch term, the viscosity is always underestimated regardless of the direction of rotation. The pinch term has often been discussed as a candidate for generation of spontaneous rotation, but this is incorrect, because the pinch term can only cause a peaking of the velocity, and cannot produce momentum. If the pinch term is proportional to the toroidal velocity, the plasma cannot spin up from the initial condition of $v_\phi = 0$ when there is no external

torque. In order to explain spontaneous rotation, a momentum sink or source near the plasma periphery is necessary.

3.3. Residual stress term

Reynolds stress-driven flow arises from the off-diagonal elements of the transport matrix. For example, the particle flux has a diffusive and a ND term which is driven by the temperature gradient or other curvature gradients. In momentum transport there should be off-diagonal terms that are driven by the temperature or pressure gradients. The relationship between the ND term of the radial flux of momentum and the ion temperature gradient is equivalent to the relationship between the residual stress and the shear flow, which has been studied from the theory point of view [164–166].

There are several approaches to study off-diagonal terms. NBI modulation experiments have been applied to distinguish diffusive and ND terms due to the residual stress. Since the residual stress is sensitive to the symmetry breaking of the turbulence, ECH has also been applied to change the turbulence (for example from an ITG mode to a trapped electron mode (TEM) dominant state) in ASDEX-U [167, 168], which is also expected by theoretical modelling. Furthermore, zero rotation plasmas with unbalanced torque give direct experimental evaluation of the intrinsic torque due to the residual stress, because both the diffusive and pinch terms almost vanish in these experiments in DIII-D [169] and LHD [170]. Rotation reversal (spontaneous change from co- to counter-rotation or vice versa during density, current or magnetic field scans with constant torque input) cannot be explained by a pinch term, but by the residual stress, which is sensitive to collisionality. The origin of the residual stress is expected to be localized near the plasma edge and more sensitive to the temperature gradient rather than the pressure gradient, based on the experiments in TJ-II [171, 172] and Alcator C-Mod.

The first experiment isolating the off-diagonal terms of the momentum matrix was performed in JFT-2M [173] and later in JT-60U [174]. In order to distinguish the diffusive and ND terms, transport analysis in the transient phase is necessary. The JFT-2M tokamak was equipped with two NBIs, one co- and the other counter-NBI. By exchanging the beams during the discharge, the plasma rotation changed its sign from co- to counter-rotation or counter- to co-rotation, and the momentum transport was analysed in the transient phase just after the NBI was exchanged, within the momentum confinement time scale. Figure 24 shows the relation between the radial flux and the gradient of toroidal momentum for the discharges when the direction of the NBI was reversed from co- to counter- (open circles) and from counter- to co- (closed circles), until the rotation velocity reached the steady-state value in 100 ms. The time resolution of the rotation measurements with charge exchange spectroscopy was 16.7 ms (60 Hz), which is fast enough to evaluate the change in momentum flux due to $n(\partial v_\phi / \partial t)$.

The relation between the momentum flux and momentum gradient plotted in figure 24(*a*) clearly shows that there is finite momentum flux even at zero momentum gradient and finite offset velocity gradient even at zero momentum flux. This is clear and direct evidence of a ND term of the
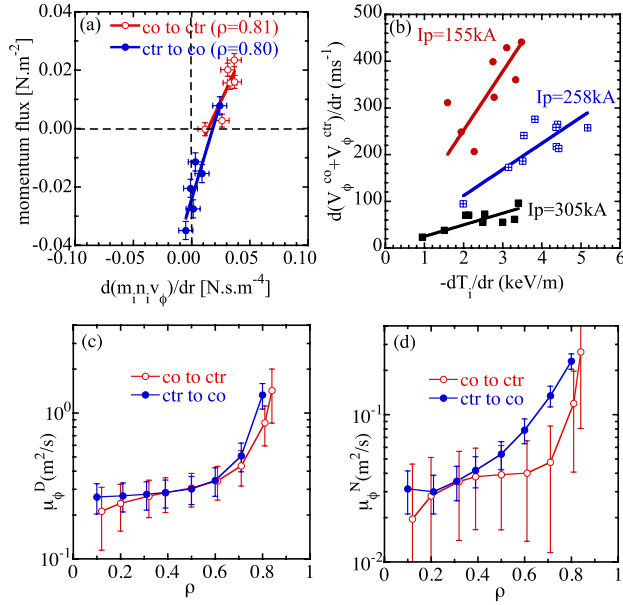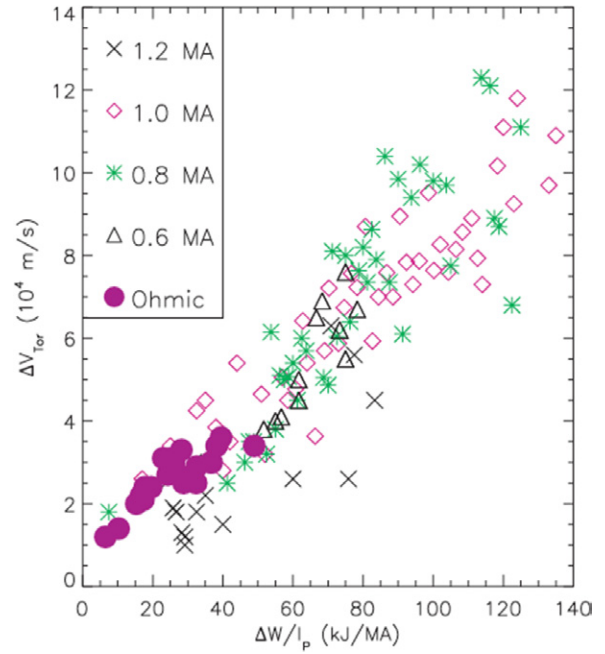
Figure 24. (*a*) Radial flux of toroidal momentum as a function of the gradient of toroidal momentum for the discharges when the direction of the NBI is reversed from co- to counter-(open circles) and from counter- to co-(closed circles). (*b*) ITG dependence of offset rotation gradient. Radial profiles of momentum viscosity coefficient in (*c*) diffusive term and in (*d*) ND term in JFT-2M. (From figures 3, 4 and 7 in [175].) Reproduced with permission from Ida K. *et al* 1998 *J. Phys. Soc. Japan* **67** 4089. Copyright 1998 by the Physical Society of Japan.

Figure 25. (*a*) Change in toroidal rotation velocity (the difference between the H-mode and pre-H-mode values) as a function of the change in plasma stored energy normalized to plasma current for ohmic and ICRF (with on-axis heating) H-modes in Alcator C-Mod [176]. Reproduced with permission from Rice J.E. *et al* 2001 *Nucl. Fusion* **41** 277. Copyright 2001 IAEA Vienna.

momentum transport and intrinsic rotation. Since the ND term is equivalent to the offset rotation gradient, the parameter dependence of the ND term was investigated using the disparity of rotation gradients between co-NBI and counter-NBI, which is essentially the same as the offset velocity gradient. As seen in figure 24(*b*) the offset rotation gradient was found to be proportional to the ITG and its slope depends on the plasma current [175]. The temperature gradient and plasma current dependence is quite consistent with the Rice scaling (see figure 25 [176] described later). Since the ND term, μ^{N}, is proportional to the ITG, it can be expressed as the coefficient of ∇T_{i}

$$\langle \tilde{v}_r \tilde{v}_\phi \rangle = -\mu_\perp^{\mathrm{D}} \nabla v_\phi + \mu_\perp^{\mathrm{N}} (v_{\mathrm{th}}/T_{\mathrm{i}}) \nabla T_{\mathrm{i}}, \qquad (9)$$

where v_{th} is the thermal velocity. The coefficient of the diffusive term, μ^{D}, is derived from the slope of the momentum flux to the momentum gradient, while the coefficient of the non-diffusive term, μ^{N}, is derived from the offset of the momentum flux. The diffusive and non-diffusive coefficients in the co-rotation plasma (after the NBI exchange from counter-NBI to co-NBI) is consistent with the counter-rotation plasma (after the NBI exchange from co-NBI to counter-NBI). This experiment shows that the ND term always contributes to the intrinsic rotation in the counter-direction regardless of the direction of the rotation itself, while the pinch term described above changes sign depending on the direction of the rotation itself. The coefficient of the ND term, μ^{N}, has an inverse dependence on plasma current, $\propto 1/I_{\mathrm{p}}$.

Co-current central impurity toroidal rotation has been observed in Alcator C-Mod plasmas with on-axis ICRF heating

[176]. The rotation velocity increases with plasma stored energy and decreases with plasma current. Figure 25 shows the parameter dependence of the change in the toroidal rotation velocity on the change in stored energy and plasma current. The ohmic values are all shown as purple circles, unseparated in plasma current, while the ICRF points are indicated by different symbols for the various plasma currents: black crosses for 1.2 MA, purple diamonds for 1.0 MA, green asterisks for 0.8 MA and black triangles for 0.6 MA. The experimental results clearly show that the intrinsic rotation has a linear dependence on stored energy. It is not clear whether the temperature gradient or pressure gradient contributes to the intrinsic rotation in the scaling of stored energy. In order to clarify whether the pressure gradient $\mathrm{d}p_{\mathrm{i}}/\mathrm{d}r$ or temperature gradient $\mathrm{d}T_{\mathrm{i}}/\mathrm{d}r$ is more important for intrinsic rotation, a more detailed analysis is necessary. (This issue will be discussed later.) The experimental results in Alcator C-Mod are quite consistent with the experiments in JFT-2M and strongly support the existence of a ND term which is proportional to the pressure or temperature gradient, and the inverse of the plasma current.

More clear evidence of the ND term (in addition to the pinch term) would be zero toroidal rotation with unbalanced torque input, where there is no possibility for the contribution of the pinch term because of zero rotation. By adjusting the number of co- and counter-NBI, (and beam power) the plasma rotation can be zeroed out (in DIII-D [177]) or almost zero (in LHD [178]). Figure 26(*a*) shows the toroidal rotation frequency profile during a phase where there are three neutral beam sources: one co- (∼2.5 MW) plus two counter- (∼5 MW) in DIII-D plasmas. Despite the fact that there is one net counter source being applied, the rotation is basically zero
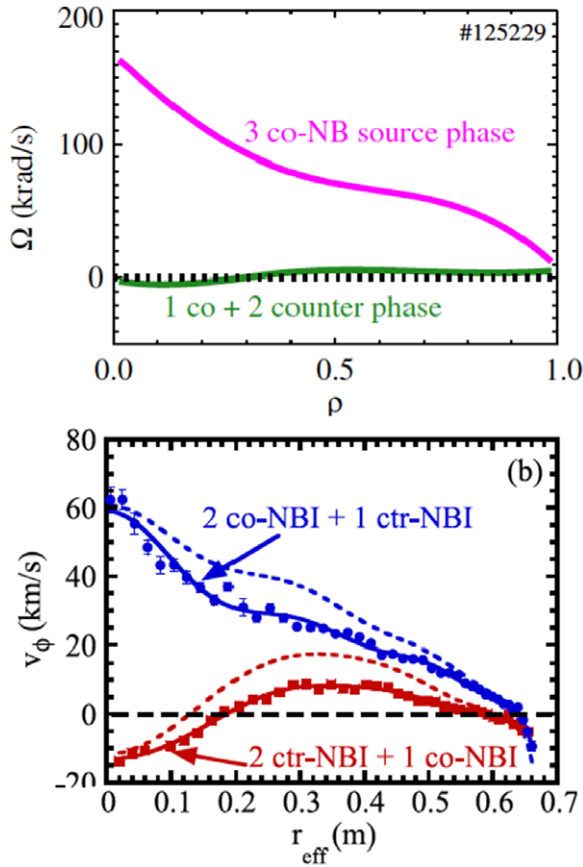
Figure 26. (*a*) Radial profiles of toroidal angular speed with 1 co- + 2 counter-neutral beam (NB) injection and 3 co-NBI in DIII-D and (*b*) radial profiles of toroidal rotation velocity with 1 co- + 2 counter-NBI and 2 co- + 1 counter-NBI in LHD. The dashed lines in (*b*) are toroidal rotation velocity profiles of main ions where the difference of rotation between the impurity and the main ion is evaluated with a neoclassical formula for the heliotron configuration. (From figure 3 in [177] figure 1 in [178].) Reproduced with permission from Ida K. *et al* 2010 *Nucl. Fusion* **50** 064007. Copyright 2010 IAEA Vienna.

Figure 27. Radial profiles of the cross correlation between parallel and radial fluctuating velocities and the production term (P) at different plasma densities in TJ-II plasmas near the LCFS. (From figures 3 and 4 in [179].) Reproduced with permission from Goncalves B. *et al* 2006 *Phys. Rev. Lett.* **96** 145001. Copyright 2006 by the American Physical Society.

across the entire plasma profile. This rotation profile is constant for several hundred milliseconds while these beams are being applied. In the case where the rotation profile is zero everywhere across the profile and not evolving, there are no terms that are proportional either to the velocity or the gradient of the velocity, and in this experiment there should be ND terms relating to the anomalous source of torque (residual stress), which balances the torque from the unbalanced NBI. The magnitude of the anomalous source of torque is comparable to the torque of one-NBI with the beam power of ~ 2.5 MW and integrated torque of ~ 3 Nm.

The dotted lines in figure 26(*b*) are the radial profiles of main ions inferred from the measured carbon rotation, and the measured ion temperature and density profiles from LHD. Since the toroidal rotation of main ions is shifted towards co-rotation, the intrinsic rotation becomes larger if it is evaluated for main ions and not impurities. (The difference between main and impurity ion rotation can be more significant in the case of ITBs, which will be discussed later.) It is interesting that the significant ND term, which is comparable to the flux due to a single beam source, is also observed in helical

plasmas. Although the magnitude of the intrinsic rotation itself is smaller in helical plasmas due to the large parallel viscosity, the magnitude of the intrinsic torque is comparable to that in tokamaks. This fact suggests that the existence of significant residual stress in helical plasmas is similar to that in tokamaks.

Because the simple collision process cannot produce parallel flow, symmetry breaking of the turbulence that propagates in the co-direction $k_\| > 0$ and that in the counter-direction $k_\| < 0$ is required. In this process the turbulence acts like an intermediary to produce toroidal torque from the radial force (∇T_i or ∇P_i). The Reynolds stress is a strong candidate for driving spontaneous rotation, but the Reynolds stress itself creates only the gradient of net flow. Therefore, the boundary condition, i.e. exhaust of momentum at the LCFS, is important. Radial profiles of the parallel–radial Reynolds stress component, proportional to the cross correlation between parallel and radial fluctuating velocities, has been measured in the plasma boundary region of the TJ-II stellarator [179]. Experimental results show the existence of significant parallel turbulent forces at plasma densities above the threshold value to trigger perpendicular $E \times B$ sheared flows, as seen in figure 27. Figure 27(*a*) shows the radial profiles of the cross correlation between parallel and radial fluctuating velocities in TJ-II plasmas near the LCFS at different plasma densities. The radial structure of $\mathrm{d}\langle \tilde{v}_r \tilde{M}_\| \rangle / \mathrm{d}r$ changes with increasing plasma density; the level of cross correlation increases for

plasma densities ($\sim 0.6 \times 10^{19}\,\mathrm{m}^{-3}$) above the threshold value to generate $E \times B$ sheared flows.

The appearance of gradients in this quantity is due to both radial variations in the level of fluctuations and in the cross-phase coherence between fluctuating radial and parallel velocities. Gradients in $\mathrm{d}\langle \tilde{v}_r \tilde{M}_{||} \rangle / \mathrm{d}r$ mainly appear at the radial location where perpendicular and parallel sheared flows are developed. From the radial derivative of the mean parallel velocity and the radial–parallel component of the Reynolds stress, the radial–parallel contribution to the production of turbulent kinetic energy (P) is computed as

$$P = -\langle \tilde{v}_r \tilde{M}_{||} \rangle \mathrm{d}M_{||}/\mathrm{d}r. \tag{10}$$

This result suggests that parallel turbulent forces are relevant in momentum dynamics during the development of sheared flows in the proximity of the LCFS. Two different signs are found in P, thus implying that the turbulence can act as an energy sink ($P > 0$) for the mean flow or energy source ($P < 0$) near the shear layer. These turbulent parallel forces are mainly localized at the radial location where sheared flows are developed. The momentum sinks and sources near the LCFS are crucial candidates for the driving mechanism of spontaneous/intrinsic rotation, because the plasma cannot rotate spontaneously without a momentum sink or source. This experiment demonstrates that the residual stress parallel to the magnetic field is one of the candidates for a sink or source of parallel flow at the plasma edge and hence can explain the reversal of intrinsic rotation during the density scan. The comparison of measured Reynolds stress with that predicted by the theoretical model should be investigated in the future. Associated with the formation of ITBs, an intrinsic torque towards the counter-direction is commonly observed in tokamaks. This intrinsic torque contributes to a reduction in the co-rotation which exists before the formation of the ITB or an increase in the counter-rotation in the region of sharp temperature gradient and $E \times B$ shear, which then contributes to the formation of a strong ITB. In plasmas with ITBs, the toroidal rotation also plays an important role in turbulence suppression [180, 181].

Spontaneous/intrinsic rotation is expected to increase in the region of transport barriers, such as in the pedestal region in H-mode plasmas and in the ITB region where a large $E \times B$ shear exists. A non-monotonic feature appears in measured toroidal velocity profiles of the carbon impurity near the radius of strongest ITG, which is called a 'notch' structure. This 'notch' structure is usually observed in the carbon impurity, but not in bulk ions. It is therefore important to evaluate both impurity and bulk plasma rotation in the ITB region. Figure 28(a) shows the radial profile of toroidal rotation velocity of carbon ions measured with charge exchange recombination spectroscopy, and the hydrogenic toroidal velocity $V_{\phi i}$, obtained by adding the calculated neoclassical parallel velocity difference to $V_{\phi x}$ in TFTR ITB plasmas [182]. It is interesting that the hydrogenic toroidal velocity $V_{\phi i}$ is essentially monotonic, which is due to the significant contribution of the diamagnetic drift (first term on the RHS of equation (5)). The monotonic profile of hydrogenic toroidal rotation does not imply a monotonic $E \times B$ profile. The $E \times B$ profile should also have a 'notch' structure, similar to the carbon rotation profiles. It should be noted that the
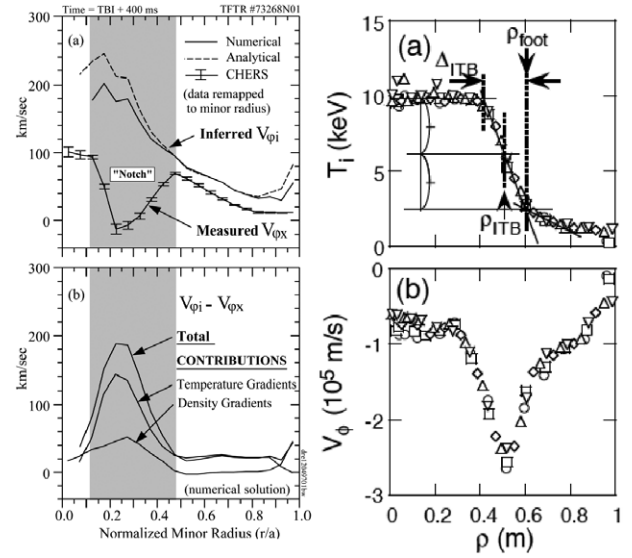

Figure 28. The velocity profile notch in TFTR 40% tritium, 30 MW quasi-balanced NBI, shown on the outer midplane. (*a*) The carbon toroidal velocity $V_{\phi x}$ measured by charge exchange recombination spectroscopy. (*b*) The toroidal velocity difference $V_{\phi i} - V_{\phi x}$ from the numerical solution. Radial profiles of ion temperature and toroidal rotation velocity obtained by jogging the plasma position from JT-60U. Different symbols indicate different times during this process. (From figure 1 in [182] and figure 1 in [185].) Reproduced with permission from Sakamoto Y. *et al* 2001 *Nucl. Fusion* **41** 865. Copyright 2001 IAEA Vienna.

turbulence suppression is due to the $E \times B$ shear, not the bulk rotation shear. The toroidal velocity difference $V_{\phi i} - V_{\phi x}$ from the numerical solution, the separate contributions of the thermal hydrogenic density and temperature gradients, and the analytical result are also plotted. These results show that the difference is mainly determined by the ITGs as predicted by neoclassical theory. The difference in toroidal rotation velocity between two impurity species measured in quiescent H-mode plasmas with a double transport barrier (QDB) in DIII-D also show good agreement with that predicted by neoclassical theory [183]. However, recent direct measurements of bulk ion rotation from D_α show that differences between core deuteron and carbon rotation in H-mode plasmas and with ITBs are inconsistent with the sign and magnitude of the neoclassical predictions [184].

Similar results are also reported in the ITB plasmas of JT-60U [185], and are shown in figure 28(*b*). In these plasmas, the large ITG region is located at $\rho = 0.4$–0.6, while the 'notch' structure has a peak in the counter-direction at $\rho = 0.5$. The appearance of the 'notch' structure exactly at the ITB region observed in JT-60U is almost identical to that observed in TFTR. The velocity difference between bulk and impurity ions would be important for evaluation of the intrinsic rotation, because in most cases the toroidal rotation velocity is measured with carbon. This velocity difference therefore causes an underestimation of intrinsic rotation in the co-direction and an overestimate in the counter-direction.

One of the important issues of the ND term relating to the residual stress is whether it is driven by the ion temperature ($P_\phi/(n_i m_i) \propto v_{th} \nabla T_i/T_i$) or pressure ($P_\phi/(n_i m_i) \propto v_{th} \nabla p_i/p_i$) gradients, where P_ϕ is radial flux of toroidal
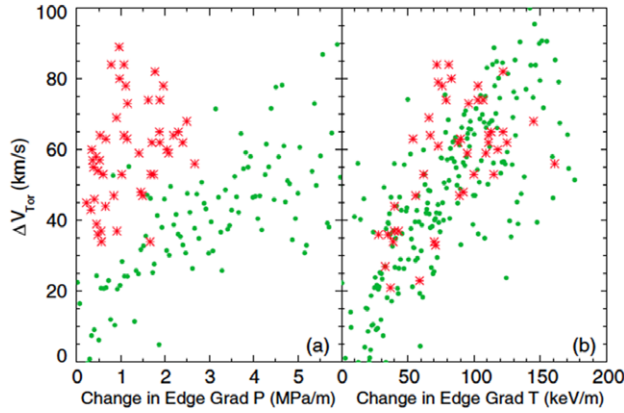
Figure 29. The change in the core rotation velocity as a function of the change in the pedestal ∇P (*a*) and pedestal ∇T (*b*) for H-mode (green dots) and I-mode (red asterisks) plasmas in Alcator C-Mod. (From figure 5 in [186].) Reproduced with permission from Rice J.E. *et al* 2011 *Phys. Rev. Lett.* **106** 215001. Copyright 2011 by the American Physical Society.

momentum [178]. The experimental results in JFT-2M discussed in figure 24 suggest the ND term is proportional to the ITG. In both experiments the distinction between temperature and pressure gradients was unclear because both gradients are strongly coupled. In LHD the behaviour of intrinsic rotation was investigated after pellet injection, where the pressure gradient is constant but the ITG increases during the density decay phase [178]. The intrinsic rotation shear (and intrinsic rotation in the co-direction) increases after the pellet injection, while the ion pressure gradient is constant in time, and the ITG increases. After the steady-state phase of the ITG, the intrinsic rotation shear keeps increasing while the ion pressure decreases. This result suggests that intrinsic rotation in the co-direction is driven by the ITG and not by the pressure gradient. It also implies that the ion pressure gradient may contribute to the rotation in the counter-direction because the co-rotation increases as the ion pressure gradient decreases. This would be due to the neoclassical effect as described above, because the ion pressure gradient always contributes to counter-rotation for impurities.

More clear evidence that the ND term is driven by the ITG is demonstrated in the intrinsic rotation measurements in Alcator C-Mod [186]. When there is no external torque, the diffusive term and ND term are balanced as $\mu_\perp^D \nabla v_\phi = \mu_\perp^N (v_{th}/T_i)\nabla T_i$ (or $\mu_\perp^N (v_{th}/p_i)\nabla p_i$) and the intrinsic rotation at the pedestal top is determined by the ion temperature or the pressure gradient as $\Delta v_\phi^{PED} = W\nabla v_\phi \propto \nabla T_i$ (or ∇p_i), where W is the pedestal width. Figure 29 shows the change in the core rotation velocity as a function of the temperature and pressure gradients at the pedestal in H- and I-mode plasmas. Because of the larger density gradient in the pedestal region in H-mode compared with I-mode, the pressure gradient is larger in H-mode than that in I-mode plasmas for a given ITG. When the intrinsic rotation is plotted as a function of temperature gradient, the intrinsic rotation both in H-mode and I-mode shows a linear dependence on ∇T_i more clearly than that plotted as a function of pressure gradient. Comparison of the intrinsic rotation in H-mode and I-mode plasmas shows that the drive of the intrinsic rotation is the edge temperature gradient rather than pressure gradient, which supports the hypothesis
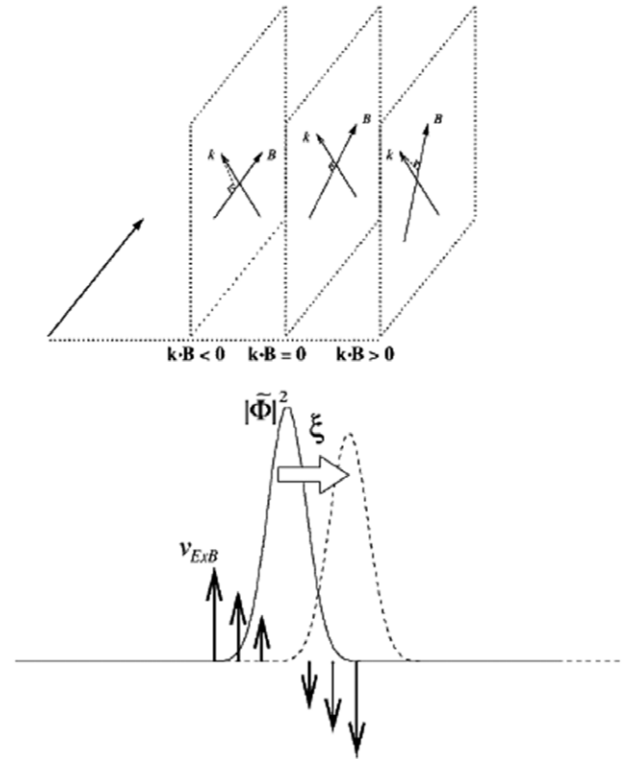
Figure 30. Shift of the intensity fluctuation profile due to $E \times B$ shear. (From figure 2 in [189].) Reproduced with permission from Gürcan O.D. *et al* 2007 *Phys. Plasmas* **14** 042306. Copyright 2007 AIP Publishing LLC.

that the intrinsic rotation is driven by the residual stress. These results are consistent with the linear proportionality of intrinsic torque to temperature gradients recently predicted by the gyrokinetic simulation of ITG or CTEM turbulence [187, 188].

The following mechanism, where the net parallel flow is accelerated by turbulence, has been proposed for the intrinsic rotation drive. Symmetry breaking of turbulence driven by $E \times B$ shear generates the parallel Reynolds stress, which contributes to nonzero parallel flow. As seen in figure 30, $E \times B$ shear in the plasma induces the parallel component of wave momentum for the eigenmodes, which propagates perpendicular to the magnetic field. This parallel component is positive on the side where the angle between the magnetic field B and k is slightly below 90°, while it is negative on the other side where the angle is above 90°. When the pressure and turbulence are constant in space, the eigenmodes described above are symmetric and there is no net parallel Reynolds stress.

The $E \times B$ shear causes a shift of fluctuation intensity from the resonance surface, in which the centroid displacement is proportional to the $E \times B$ shear of $\partial v_\perp / \partial r$. The parallel stress can be written as [189]

$$\langle \tilde{v}_r \tilde{v}_{||} \rangle = -Re \sum i v_{th}^2 \left(\frac{\Omega_i}{\omega_k}\right) \rho_i^2 k_\perp^2 \left[\frac{\rho_i}{v_{th}} \frac{\partial v_{||}}{\partial r} -\alpha \left(\frac{v_{th} k_\perp}{\omega_k} \frac{\rho_i}{P} \frac{\partial P}{\partial r} - 1\right) \frac{\rho_s}{L_s} \frac{L_n}{c_s} \frac{\partial v_\perp}{\partial r}\right] \left|\frac{e\tilde{\Phi}_k}{T_i}\right|^2, \quad (11)$$

where $v_{||}$ and $\tilde{v}_{||}$ are the parallel mean velocity and its fluctuating value, respectively, and Ω_i, ω_k, ρ_i and P are the

ion-cyclotron frequency and turbulence frequency with the wave number $k_\perp$, ion Larmor radius and plasma pressure. c_s is the ion sound velocity, $\rho_s^2 = c_s^2/\Omega_i^2$ and L_n and L_s are the scale lengths of the density profile and magnetic shear, defined as $(\nabla n/n)^{-1}$ and $Rq/\hat{s}$, where $\hat{s}$ is magnetic shear ($\hat{s} = (r/q)(\partial q/\partial r)$). The magnitude and sign of the coefficient, α, is determined by the type of turbulence. For example it is positive for electron drift wave (DW) turbulence and negative for ITG driven turbulence [189]. The first term is the diagonal diffusive flux due to the parallel flow shear and the second term is the ND off-diagonal flux due to perpendicular flow shear. The first term is the parallel component of Reynolds stress due to the radial shear of parallel flow itself and the second term is the ND term due to the coupling of the pressure gradient, $E \times B$ shear and fluctuations [190].

This effect may have an analogy to the diamagnetic drift flow, where the gyro-motion under the pressure gradient produces an apparent rotation (not the rotation of guiding centres of gyro-motion). The magnetic shear $\hat{s}$ and $E \times B$ shear produce the parallel component of wave momentum and each of the eigenmodes has a finite size in the plasma where the pressure gradient exists. Therefore, the key parameters for this effect are (1) the magnetic shear, (2) the $E \times B$ shear with the scale length small enough, comparable to the size of the eigenmode of the turbulence, (3) the pressure gradient, (4) the radial gradient of fluctuations $\partial \tilde{\Phi}_k/\partial r$ [191], which is not included in this formula and (5) up–down asymmetry of the equilibrium field, which has been in observed in TCV [192]. The role of magnetic and $E \times B$ shear in this model is crucial and also consistent with the fact that the intrinsic rotation is often observed in plasmas with transport barriers where large $E \times B$ shear is expected, although the turbulence itself is somewhat (of course not completely) suppressed.

An important difference between the pinch model and residual stress is the sign dependence. In the residual stress model, the sign of the ND term (also the direction of the intrinsic rotation) depends on the type of turbulence mode, magnetic shear, $E \times B$ shear and the phase velocity of the fluctuations. In contrast, the sign dependence of the pinch term is more complicated. Although the pinch term due to TEP [161] and the Coriolis force [162] is simply determined by the sign of the rotation itself, there is a contribution to the pinch velocity that reverses with the nature of the instabilities that underlie the turbulence. For example, the curvature-driven thermal pinch (thermoelectric pinch) can be inwards or outwards, depending on the mode-propagation direction [18, 145]. It should be noted that the pinch term vanishes when the toroidal flow is zero in the middle of flow reversal. Therefore, flow reversal cannot be explained by the pinch term, and the residual stress is the most plausible candidate for the mechanism of flow reversal, which will be discussed in section 4.

It should be noted that there are alternative explanations for the linear relation between the intrinsic rotation and the temperature gradient observed near the pedestal region. This is because the boundary effect (discussed in the next section) might play an important role in determining the intrinsic rotation, apart from the intrinsic rotation observed in the ITB region, as observed in JT-60U, TFTR and LHD. Thermal ion orbit loss to the X-point is one of the important mechanisms

that can affect the edge intrinsic rotation. Another important mechanism is the pinch velocity relating the density gradient. Further research for the contribution from the change in the thermal ion orbit loss to the X-point associated with the transition to H- or I-mode and the pinch contribution due to the density gradient is necessary in order to confirm the hypothesis described above.

3.4. Kinetic stress

Recently the core rotation was observed to respond to the emergence of a strong edge co-current rotation layer, which appears to be at least partially created by purely kinetic processes in DIII-D [193]. Strong kinetic stresses are required to explain the net inward transport of toroidal momentum from the edge layer into the core. The existence of kinetic stresses is confirmed by full-f gyro-kinetic codes that can treat the plasma edge, which predict an edge co-rotation layer. The kinetic stress is a possible mechanism which can explain the effect of the plasma boundary on intrinsic rotation.

Intrinsic rotation has been found to depend strongly on magnetic configuration, such as upper single null (USN), lower single null (LSN), double null (DN) and the limiter configuration [194], and the magnitude of the intrinsic rotation also depends on the ∇B direction [195]. Discharges with an USN have significantly stronger intrinsic rotation in the counter-direction than those in the LSN configuration, when the ion $B \times \nabla B$ drift is downwards. The rotation depends very sensitively on the distance between the primary and secondary separatrixes in near double null plasmas, The rotation depends sensitively on the balance between the upper and lower null, and plays a crucial role in the H-mode power threshold. These experiments suggest that there is a strong connection between core intrinsic rotation and scrap-off layer flows [196]. At the plasma boundary, there are other physics processes that may cause the intrinsic torque and rotation other than the residual stress described in the previous section. For example, the interaction between the radial displacements of passing-ion orbits and turbulence inhomogeneity results in residual stress and corresponding pedestal-top intrinsic rotation [197]. Turbulent stresses and flows inside the separatrix of tokamak H-mode plasmas have been measured using Langmuir probes at DIII-D [193]. Although the intrinsic co-rotation layer is observed near the separatrix, the measured Reynolds stress is too small to drive the observed intrinsic rotation. These measurements also imply the existence of a large kinetic stress in addition to the Reynolds stress discussed in section 3.

An edge loss cone in velocity space was previously considered as a possible mechanism to generate an edge rotation source under intrinsic rotation conditions. The impact of thermal ion orbit losses on the interpretation of the pedestal transport has been recognized recently. Simulation models are presented for treating ion orbit loss effects in interpretive fluid transport calculations for the tokamak edge pedestal [198, 199]. A complete description of thermal ion orbit losses to the X-point as a driver of intrinsic rotation was reported. The kinetic stress due to thermal ion orbit loss may play an important role and make significant contributions to the intrinsic rotation, especially near the plasma boundary where the thermal orbit loss to the X-point occurs. The collisionless
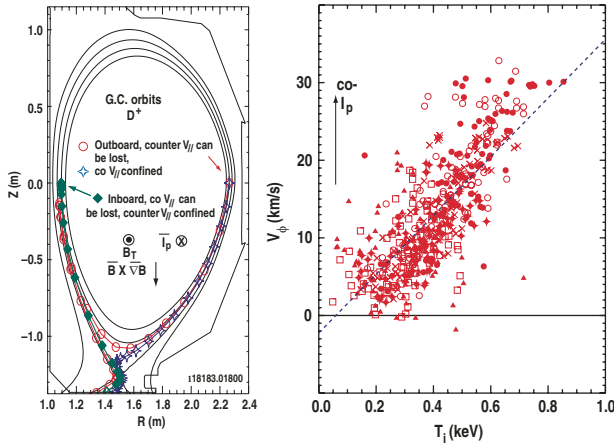
Figure 31. Equilibrium flux surface and the intrinsic toroidal rotation velocity as a function of ion temperature near the top of the pedestal in DIII-D. (From figures 8 and 7 in [109].) Reproduced with permission from deGrassie J.S. *et al* 2009 *Nucl. Fusion* **49** 085020. Copyright 2009 IAEA Vienna.

loss orbit from the edge to the divertor exists only near the LCFS within 1–2 cm, and the unbalanced mechanical momentum remains in the edge pedestal region. Figure 31 shows equilibrium flux surfaces and three guiding centre loss orbits of counter-I_p velocity ions starting from the outboard midplane (circle, cusp symbols) and co-I_p velocity ions starting at the inboard midplane (diamonds) in the vicinity of the X-point. The barely trapped orbits (circles) have sufficient time to fall into the X-point region and counter-I_p velocity ions starting from the outboard midplane can be lost. The more deeply trapped orbits (cusps) have greater energy and thus a greater vertical drift velocity to escape, and can be confined. The inboard co-I_p velocity ions (diamonds) are in a mirror situation and can be lost. Calculations with full-f numerical simulations have been developed in order to evaluate quantitatively the loss of co- and counter-I_p velocity ions. The XGC1 edge loss simulation code demonstrates that there is a robust spontaneous co-current toroidal plasma rotation source in the far scrape-off layer plasma due to the wall sheath effect. As the edge pedestal width becomes narrower, the co-current rotation in the far scrape-off layer becomes weaker, but there appears a stronger co-current rotation in the pedestal top/shoulder from the X-point orbit loss effect, possibly providing a co-rotation boundary condition to the core plasma [200]. These simulation results are consistent with the experimental measurements in DIII-D, where the intrinsic rotation in the co-I_p direction increases linearly as the ion temperature is increased [109].

The intrinsic toroidal rotation velocity as a function of ion temperature at various locations (R = 2.221, 2.234, 2.251, 2.265, 2.271, 2.277 m) near the top of the pedestal in DIII-D is also plotted in figure 31. Although there is more scatter in the correlation, it is still clear that the toroidal rotation, V_ϕ, is roughly proportional to the ion temperature, T_i, although it might appear that a higher power than linear in T_i could be indicated. It should be noted that the relation between intrinsic rotation and ion temperature near the plasma edge observed in DIII-D is similar to that observed in Alcator C-Mod. The kinetic stress is an alternative explanation in addition to the residual stress for the driving mechanism of intrinsic rotation

at the pedestal (which is roughly proportional to temperature). Recent Mach probe measurements of the bulk ion toroidal velocity near the LCFS in DIII-D [193] are consistent with the existence of a loss-cone distribution in velocity space. This model has been extended into the scrape-off layer, takes into account limiting surfaces and is also extended to include the effect of a uniform radial electric field with magnitude and sign relevant for measurements in the edge of DIII-D H-mode conditions [201].

4. Important issues for future study

Regarding intrinsic rotation, there are various interesting phenomena observed which are due to the non-linearity of the residual stress. Flow reversal and the flip of intrinsic torque cannot be explained by the pinch model and provide important evidence for the residual stress. In this section, experimental observations of flow reversals, hysteresis in intrinsic rotation and the relation to non-local transport are discussed.

4.1. Flow reversal

Flow reversal has been observed both in tokamak plasmas in TCV [202], Alcator C-Mod [203, 204] and ASDEX Upgrade [205] and helical plasmas. Reversal of the toroidal rotation velocity is an interesting phenomenon in toroidal plasmas, and understanding the cause is important for clarifying the driving mechanism of the ND term of the momentum transport [206, 207]. This is similar to the L/H transition in energy transport, where significant improvement in the understanding of heat transport has developed after the discovery of H-mode. Flow reversal to the direction anti-parallel to the $E_r \times B_\theta$ drift direction was first found in plasmas associated with a significant decrease in collisionality in CHS [208, 209]. As seen in figure 32, after the second ECH is applied to the low density co-injected NBI target plasma, the electron temperature increases from 0.2 keV (L-mode) to 2 keV (hot electron mode) with the decrease in electron density from 0.6×10^{19} to 0.3×10^{19} m^{-3}. The large poloidal rotation velocity in the ion diamagnetic direction (positive radial electric field) appears with the peak at $\rho \sim 0.5$ while the poloidal rotation is almost zero in the L-mode plasma. The toroidal rotation velocity is in the co-direction (same direction of the NBI) in L-mode. When the plasma collisionality drops following the second ECH pulse, the toroidal rotation changes its sign from co- to counter-rotation. The momentum flux due to the ND term is even larger than the momentum flux due to tangential NBI. This is a plasma where the electron temperature is much larger than the ion temperature by an order of magnitude, $T_e \approx 10T_i$, and turbulence driven by the electron temperature gradient would be dominant. It should be noted that changes in the poloidal rotation and the $E \times B$ flow precede the flow reversal in the toroidal rotation. This fact suggests the importance of the radial electric field and supports the residual stress model described above. In this experiment there were no turbulence measurements; however, the type of the turbulence should differ because of the significant change in collisionality by two orders of magnitude.

Toroidal flow anti-parallel to the $E_r \times B_\theta$ drift direction is observed (although the toroidal flow measured is parallel
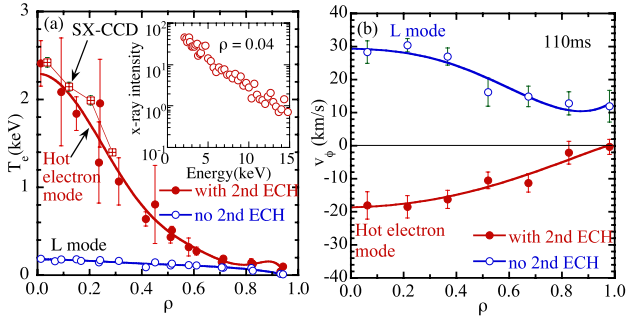
Figure 32. Radial profiles of (*a*) electron temperature averaged over 70–140 ms measured with YAG Thomson scattering and a spectrum of x-ray emission at $\rho = 0.04$, and electron temperature measured with a SX-CCD camera and (*b*) toroidal flow velocity at $t = 110$ ms for the discharges with (solid circles) and without (open circles) a second ECH pulse in CHS. (From figure 1 [208].) Reproduced with permission from Ida K. *et al* 2001 *Phys. Rev. Lett.* **86** 3040. Copyright 2001 by the American Physical Society.

to the direction of the local $E_r \times B_\theta$ drift) in the hot electron mode in CHS. This is in contrast to the spontaneous toroidal flow in the direction parallel to the direction of $\langle E_r \times B_\theta \rangle$ drift in tokamak plasmas. This toroidal flow can be large enough to overcome the toroidal flow driven by a tangentially injected neutral beam at the transport barrier. The reversal of the toroidal flow velocity with the second ECH pulse in the hot electron mode can be explained by the viscous stress, which favours flow in the minimum ∇B direction. This experiment suggests the importance of the driving force for residual stress and parallel viscosity. In CHS, flow reversal is observed only in plasmas with ECH because the collisionality is relatively high in the NBI plasmas, and no transition phenomenon is observed. However, in LHD plasmas, where the collisionality is low enough even in NBI plasmas, a clear transition from co- to counter-rotation is observed when the electron density exceeds a critical value of $1 \sim 2 \times 10^{19}$ m^{-3} without ECH [210]. Therefore, flow reversal in CHS is considered to be not due to ECH-driven flow but to the change in collisionality, which suggests a flow reversal mechanism similar to that observed in tokamak plasmas.

Flow reversal of toroidal rotation is also observed in tokamaks in the manner of transition phenomena in TCV [202]. In contrast to the experiment in CHS, the flow reversal takes place abruptly during the density ramp up, with a small change in collisionality. The toroidal rotation is observed to invert spontaneously from the counter- to co-current direction when the plasma electron density exceeds a well-defined threshold, as seen in figure 33. In this discharge the electron density increases gradually from 3×10^{19} to 7×10^{19} m^{-3}, while the electron temperature gradually decreases from 1.0 to 0.7 keV. At a threshold electron density of 6×10^{19} m^{-3}, the toroidal angular velocity flips its sign from the counter- to the co-direction on a time scale of 100 ms. The change of rotation affects the central part of the plasma. After the inversion, ω_ϕ for $\rho > 0.85$ recovers its former value. When the core rotation crosses through zero during the transient phase from counter-rotation, edge rotation in the counter-direction is observed. This edge rotation might be an indication of recoil through the conservation of angular momentum. It is an interesting observation that the direction of the intrinsic rotation is quite
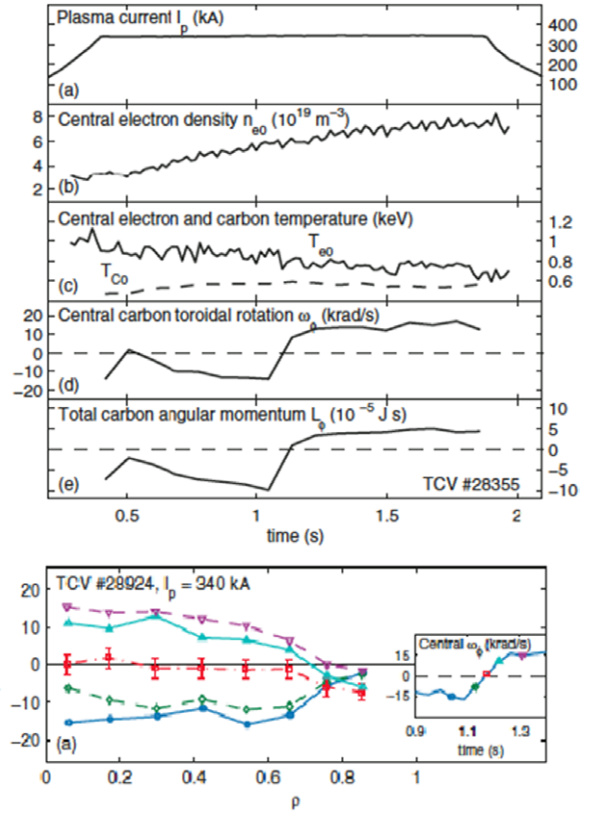
Figure 33. Characteristic time traces of discharge parameters, from top to bottom: plasma current, central electron density, central electron and carbon temperature, central carbon toroidal rotation, and total angular momentum (top). Positive values indicate flows in the ion diamagnetic direction (co-current). Rotation profiles at different times are shown in the bottom in TCV. (From figures 2 and 5 in [202].) Reproduced with permission from Bortolon A. *et al* 2006 *Phys. Rev. Lett.* **97** 235003. Copyright 2006 by the American Physical Society.

sensitive to the collisionality, and that the change in the direction of intrinsic rotation is abrupt. The onset of the residual stress which causes the flip of rotation is also abrupt, and the non-linearity of this phenomenon cannot be explained by the pinch term, where the ratio of the pinch to the diffusive term is constant. One of the candidate mechanisms to flip the rotation is a change in the turbulence mode. The simultaneous measurements of intrinsic rotation and turbulence should be very important, but which is not reported from TCV.

Similar flow reversal phenomena are observed in the Alcator C-Mod tokamak [211]. The flow reversal takes place during the density ramp up, but the direction of the flow reversal is different from that observed in TCV. Direction reversals of intrinsic toroidal rotation from the co- to the counter-direction have been observed at $t = 1.15$ s in ohmic L-mode plasmas following electron density ramps, as seen in figure 34. (The reversal of intrinsic rotation from counter- to co-rotation is observed at $t = 0.67$ s during the decay phase of the density.) Note that the plasma in C-Mod is in the diverter configuration, while the plasma in TCV (figure 33) is in the limiter configuration. The differences between these two experiments suggest that the direction of the intrinsic rotation is quite sensitive to the boundary condition: limiter or diverter configurations. Density fluctuations with k_R between 4.2 and
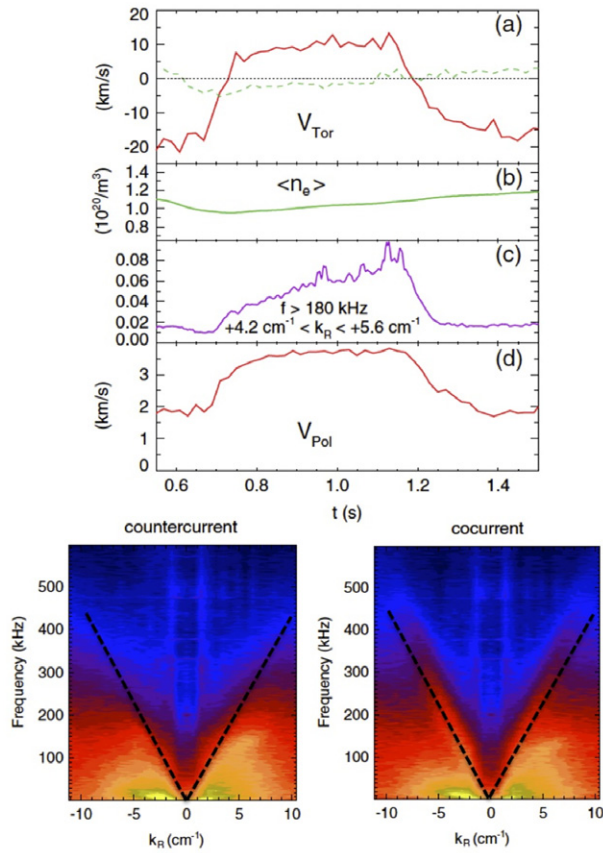
Figure 34. Time histories of (*a*) the toroidal rotation velocity at the centre (solid line) and outside of $r/a = 0.75$ (dashed line), (*b*) average electron density, (*c*) density fluctuation intensity with k_R between 4.2 and 5.6 cm^{-1} and frequency above 180 kHz and (*d*) the poloidal propagation velocity of the turbulence. At the bottom are dispersion plots of the turbulence at two different times in Alcator C-Mod. (From figures 1 and 3 in [224].) Reproduced with permission from Rice J.E. *et al* 2011 *Phys. Rev. Lett.* **107** 265001. Copyright 2011 by the American Physical Society.

5.6 cm^{-1} are measured in order to investigate the mechanism of the residual stress. The discharge which underwent two rotation reversals is with a plasma current of 1.1 MA and magnetic field of 5.4 T ($q_{95} = 3.2$), respectively. Dispersion plots $S(k, f)$ of turbulence before (0.608 s, counter-current rotation) and after (0.859 s, co-current rotation) the first rotation reversal show significant differences. High frequency turbulence ($f \sim 200$–300 kHz) with medium wave number $k_R \sim 5$ cm^{-1} is much more pronounced in the dispersion plot during the co-current rotation. This is also seen in the time evolution of the fluctuation amplitude with $f > 180$ kHz and 4.2 cm$^{-1} < k_R < 5.6$ cm^{-1}, which is in the range of TEM turbulence. This experiment implies a strong correlation between the direction of rotation and turbulence. Residual stress-driven flow is sensitive to the characteristics of turbulence; specifically the direction of the flow driven by the Reynolds stress is found to be correlated with the turbulence mode.

The flip of intrinsic torque associated with the transition of dominant turbulence between TEMs and ITG modes is also predicted by nonlinear global delta-f gyro-kinetic particle simulations [15]. Therefore, the transition of dominant

turbulence (e.g. TEM to ITG or vice versa) is one of the candidates to explain the experimentally observed flip in rotation. However, simulation with multi-turbulence is required to understand the mechanism of flow reversal, because there are many turbulent modes co-existing in the plasma [212]. Recent comparison of the experimental results with the nonlinear gyro-kinetic theory using synthetic diagnostics and the code GYRO demonstrates that changes in intrinsic rotation profiles do not correlate with changes in particle transport, and also do not correlate with changes in linear mode dominance, e.g. ITG versus TEM [213]. The reversal of intrinsic torque associated with the formation of ITBs observed in LHD shows the clear correlation between the reversal of intrinsic torque and changes in ion heat transport, but not the correlation with the transition between TEM and ITG [214].
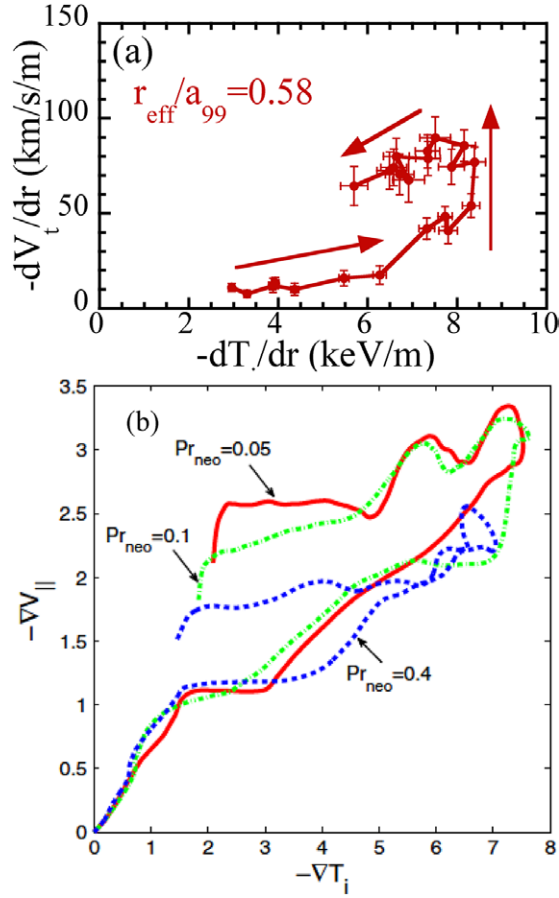
4.2. Hysteresis of intrinsic rotation

Hysteresis between the intrinsic rotation velocity gradient and the ITG (∇V_ϕ and ∇T_i) is expected in ITG-driven intrinsic rotation. This is because the residual stress driving the rotation is roughly proportional to the ITG in plasmas where ITG turbulence is dominant. These have been observed in experiments [178] and in simulations [215] of ITG turbulence with ITBs.

A clear jump of intrinsic velocity shear due to this hysteresis is observed in the stronger ITBs in LHD plasmas, where the ITG exceeds 8 keV m^{-1}, as seen in figure 35. This is a discharge with dominant co-NBI and the velocity shear near the plasma centre increases in the co-direction. Although the ITG starts to decrease in the later phase of the ITB period, the velocity gradient maintains a large value. This observation indicates that the intrinsic rotation has transition characteristics in magnitude (not the direction apart from flow reversal) and there are two states; one with small intrinsic rotation and the other with large intrinsic rotation. The control parameter for this transition seems to be the temperature gradient. It is interesting that the ND term, as well as the diffusive term, can bifurcate in momentum transport. This is in contrast to the bifurcation of only the diffusive term as has been identified in heat transport, although there is some experimental evidence of a ND term, recognized as a heat pinch [216, 217].

Figure 35(*b*) shows the relation between $-\nabla V_{\text{parallel}}$ and $-\nabla T_i$ in ITB plasmas simulated for various Pr_{neo} values. Here Pr_{neo} is the ratio between two collisional diffusivities, namely the collisional Prandtl number, which is defined as the ratio $\chi_\phi^{\text{neo}}/\chi_i^{\text{neo}}$, which is much larger in helical plasmas than that in tokamaks due to large toroidal viscosities. It clearly shows a stronger hysteresis of flow compared with the ion temperature. Indeed, flow shear undergoes less relaxation than the ion temperature and persists even after the back transition, which shows hysteresis similar to that observed in LHD. This simulation also demonstrates that the hysteresis strength decreases as Pr_{neo} increases, implying relatively stronger hysteresis of the flow gradient over the ITG.
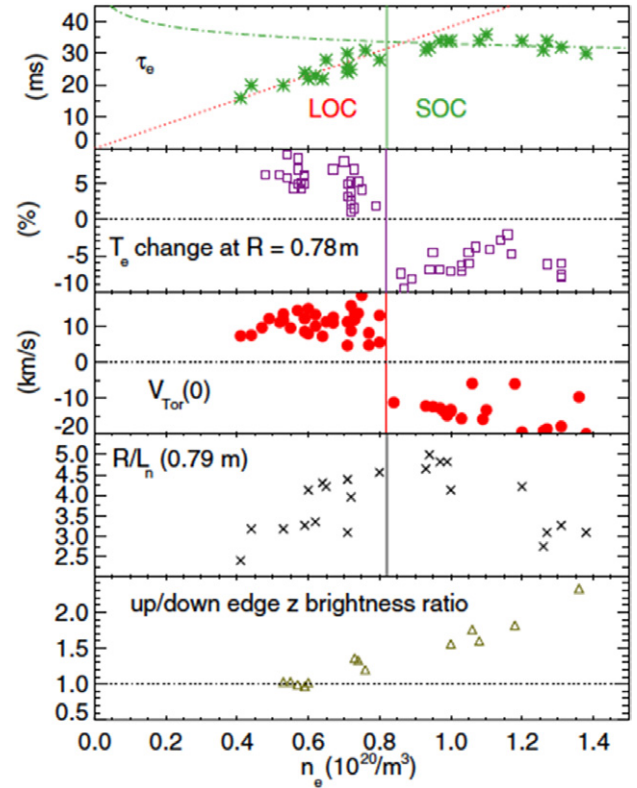
4.3. Relation to non-local transport

Recently the relation between rotation reversals and non-local response to cold pulses was experimentally observed in Alcator C-Mod [218]. Non-local phenomena have been

Figure 35. Hysteresis of intrinsic rotation velocity gradient and ITG in (*a*) experiment (LHD) and in simulation (*b*). (From figure 8 in [178] and figure 9 in [215].) Reproduced with permission from Kim S.S. *et al* 2011 *Nucl. Fusion* **51** 073021. Copyright 2011 IAEA Vienna.

Figure 36. Global confinement time, change in electron temperature after edge cooling, core toroidal rotation velocity, the inverse density gradient scale length and up/down edge impurity brightness ratio as a function of electron density in Alcator C-Mod. (From figure 11 in [218].) Reproduced with permission from Rice J.E. *et al* 2013 *Nucl. Fusion* **53** 033004. Copyright 2013 IAEA Vienna.

observed in heat transport experimentally [219–222] and also have been predicted by simulations [223]. Figure 36 shows the energy confinement time, non-local response, intrinsic rotation, density peaking and up/down edge impurity brightness in the density range where the confinement regime changes from linear ohmic confinement (LOC) to saturated ohmic confinement (SOC).

In the LOC regime the toroidal rotation is in the co-direction, while it is in the counter-direction in the SOC regime. Rises in the electron temperature (positive value) associated with the edge cooling due to impurity injection are observed only in the LOC regime, while drops in electron temperature (negative value), on the diffusion time scale, are observed in the SOC regime. For this current and magnetic field, the critical density where the non-local temperature rise disappears is $0.8 \times 10^{20} \, \mathrm{m}^{-3}$. Near this critical density, the electron density profile becomes peaked. The up/down edge impurity brightness ratio shows that the edge impurity density becomes up/down asymmetric in the SOC regime, while it is almost symmetric in the LOC regime. These observations clearly show that both the non-local response (T_e rise or drop) and sign of intrinsic rotation (co- or counter-rotation) undergoe the transition at the same critical density associated with the change in the confinement regime (LOC and SOC), where the

turbulence structure (turbulence mode) is different [224]. This experiment clearly shows the very strong connection between the appearance/disappearance of non-local response and the direction of intrinsic rotation. Since this transition occurs at a critical density which depends on q_{95} (and R), it suggests that a critical collisionality is the relevant parameter.

So far, non-local phenomena in momentum transport itself have not been identified experimentally. This is because momentum transport has a ND term and a careful analysis to identify the non-local effect is required. There are two mechanisms that may cause non-local momentum transport. It is well known that heat transport has 'non-local' characteristics, where the radial heat flux is determined by the local magnitude of the turbulence but not local plasma parameters (e.g. density, temperature and their gradients) and field parameters (e.g. radial electric field and magnetic field shear) because of the coupling between micro-, meso- and macro-scale turbulence. Therefore, both the diffusive and non-diffusive terms of the radial momentum flux driven by turbulence should have 'non-local' characteristics similar to that observed in heat transport. In experiments, it is not easy to extract the feature of 'non-local' transport because of the significant contribution of the ND terms. However, 'non-local' characteristics should be investigated with perturbation techniques in particle and momentum transport, as well as in heat transport, in order to have a comprehensive understanding of turbulent transport in toroidal plasmas.
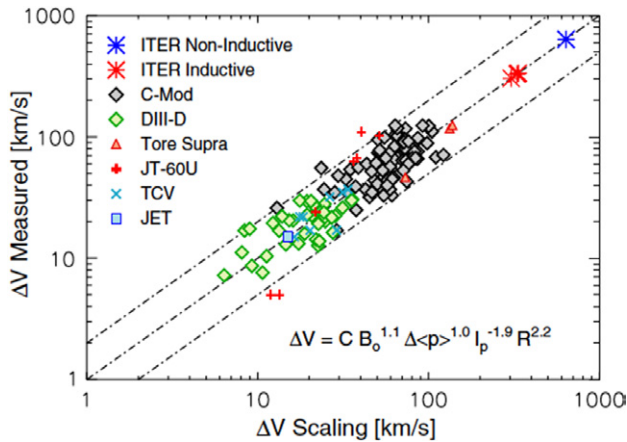
Figure 37. The measured change in the rotation velocity as a function of the scaling with $\Delta V = C B^{1.1} \Delta \langle P \rangle^{1.0} I_{\mathrm{p}}^{-1.9} R^{2.2}$. (From figure 9 in [225].) Reproduced with permission from Rice J.E. *et al* 2007 *Nucl. Fusion* **47** 1618. Copyright 2007 IAEA Vienna.

5. Predictions for intrinsic rotation

A regression analysis has been performed on the intrinsic rotation data set in H-mode and other enhanced confinement regimes from C-Mod, DIII-D, Tore Supra, JT-60U, TCV and JET, as seen in figure 37 [225]. The change in the rotation velocity measured is proportional to $C B_0^{1.1} \Delta \langle p \rangle I_{\mathrm{p}}^{-1.9} R^{2.2}$. Most of the points are within a factor of two of the scaling; some of the scatter may be due to the large variety in magnetic field ripple, error fields and/or wall conditioning in the various devices. Extrapolation to ITER predicts rotation velocities in excess of $300\,\mathrm{km\,s^{-1}}$. For an ITER discharge with $\beta_\mathrm{N} = 2.6$, an intrinsic rotation Alfvén Mach number of 0.02 may be expected, enough to suppress RWMs without any external momentum input.

Note that the scaling is not for the absolute intrinsic rotation, V, but for the increment of intrinsic rotation ΔV, and this scaling gives only the relation between ΔV and ΔP. The magnitude of the intrinsic rotation is not determined by this scaling because of the complexity of the physics involved in momentum transport. This scaling shows that the driving mechanism of intrinsic rotation is related to the magnetic field pitch, q, poloidal field, and pressure gradient, since the scaling can be re-written as $\Delta V \times B_\mathrm{p} \propto \Delta P q (R/a)^3$. Here the role of the ΔP is through an enhancement of turbulence due to the increase in the pressure/temperature gradient, while q shows the importance of magnetic field pitch and magnetic shear. This scaling shows the relation of intrinsic rotation to global plasma parameters, and the parameter dependence is not based on a physics model. Therefore, the scaling is not enough to predict the intrinsic rotation in future devices, since the driving mechanism of intrinsic rotation is complicated, and there are many observations that cannot be expressed with this scaling. For example, the change in sign of intrinsic torque such as seen in the flow reversal process during collisionality scans or the transition from L-mode to the plasmas with ITBs [214] cannot be explained by the parameter dependence of this scaling. Also in some cases, the intrinsic torque is localized near the edge pedestal where the pressure gradient is large. Although local parameters such as the pressure gradient look important, this

scaling does not include the local pressure gradient, and is only expressed by global parameters. Other intrinsic rotation scalings based on local rather than global parameters have also been developed [226].

There are many unresolved problems regarding intrinsic rotation. One of the important issues is the sign of the rotation. As seen in the reversal phenomenon, the direction of the intrinsic rotation changes its sign, even with slight changes in plasma parameters, which cannot be expressed by a global parameter scaling. The other issue is that the intrinsic rotation is very sensitive to the change in turbulence type, and also to the confinement mode, such as LOC/SOC, L-mode/H-mode or L-mode/ITB. Although the magnitude of intrinsic rotation may be sufficient in ITER, the flip in rotation is of concern, so an understanding of rotation reversals is crucial. In order to achieve stable operation in ITER, a better understanding based on the physics mechanisms of intrinsic rotation is necessary.

There are several physics issues which should be understood in order to predict the intrinsic rotation in future devices. The physics mechanism determining the direction and magnitude of intrinsic torque is still not well enough understood to give a precise prediction, although there are many experimental observations and simulations. Since the intrinsic torque is related to the symmetry breaking of turbulence, it should be correlated with the confinement regime, as well as to heat and particle transport. At the moment, the understanding of the connection among the particle pinch, intrinsic torque and non-local response of the heat transport is still phenomenological. The other remaining issue is how the angular momentum is released when the intrinsic rotation appears. It is not clear whether angular momentum is conserved by the kinetic momentum escaping from the last closed flux surface or by a change in the magnetic vector potential. Therefore, momentum transport across the LCFS (momentum exchange), which is not discussed in this review, should be addressed in future investigations.

Acknowledgments

References

[1] Groebner R. *et al* 1990 *Phys. Rev. Lett.* **64** 3015
[2] Ida K. *et al* 1990 *Phys. Rev. Lett.* **65** 1364
[3] Wagner F. *et al* 1982 *Phys. Rev. Lett.* **49** 1408
[4] Hallock G.A. *et al* 1986 *Phys. Rev. Lett.* **56** 1248
[5] Biglari H., Diamond P.H. and Terry P.W. 1990 *Phys. Fluids* B **2** 1
[6] Garofalo A.M. *et al* 2002 *Phys. Rev. Lett.* **89** 235001
[7] Takechi M. *et al* 2007 *Phys. Rev. Lett.* **98** 055002
[8] Berkery J.W. *et al* 2010 *Phys. Rev. Lett.* **104** 035003
[9] Rice J.E. 2008 *J. Phys.: Conf. Ser.* **123** 012003
[10] Shaing K.C. 2001 *Phys. Rev. Lett.* **86** 640
[11] deGrassie J.S. 2009 *Plasma Phys. Control. Fusion* **51** 124047
[12] Peeters A.G. *et al* 2011 *Nucl. Fusion* **51** 094027
[13] Coppi B. 2002 *Nucl. Fusion* **42** 1
[14] Dominguez R.R. and Staebler G.M. 1993 *Phys. Fluids.* B **5** 3876

[15] Diamond P.H. *et al* 2013 *Nucl. Fusion* **53** 104019
[16] Goldston R.J. *et al* 1981 *J. Comput. Phys.* **43** 61
[17] Diamond P.H. *et al* 2008 *Phys. Plasmas* **15** 012303
[18] Diamond P.H. *et al* 2009 *Nucl. Fusion* **49** 045002
[19] Itoh S.I. 1992 *Phys. Fluids* B **4** 796
[20] Casson F.J. *et al* 2009 *Phys. Plasmas* **16** 092303
[21] Nave M.F.F. *et al* 2010 *Phys. Rev. Lett.* **105** 105005
[22] Jackson G.L. *et al* 1986 *Phys. Rev. Lett.* **67** 3098
[23] Osborne T.H. *et al* 1994 *Plasma Phys. Control. Fusion*
     36 A237
[24] McDermott R.M. *et al* 2009 *Phys. Plasmas* **16** 056103
[25] Whyte D.G. *et al* 2010 *Nucl. Fusion* **50** 105005
[26] Ida K. *et al* 2001 *Phys. Plasmas* **8** 1
[27] Ida K. *et al* 2001 *J. Plasma Fusion Res.* **4** 36
[28] Fujisawa A. *et al* 1998 *Phys. Rev. Lett.* **81** 2256
[29] Fujisawa A. *et al* 1999 *Phys. Rev. Lett.* **82** 2669
[30] Lore J. *et al* 2010 *Phys. Plasmas* **17** 056101
[31] Baldzuhn J. *et al* 1998 *Plasma Phys. Control. Fusion* **40** 967
[32] Velasco J.L. *et al* 2012 *Plasma Phys. Control. Fusion*
     54 015005
[33] Nishimura S. *et al* 2000 *Phys. Plasmas* **7** 437
[34] Asakura N. *et al* 2000 *Phys. Rev. Lett.* **84** 3093
[35] Burrell K. *et al* 1988 *Nucl. Fusion* **28** 3
[36] Suckewer S. *et al* 1981 *Nucl. Fusion* **21** 1301
[37] Yamamoto S. *et al* 1983 *Proc. 9th Int. Conf. on Plasma*
     Physics and Controlled Nuclear Fusion Research
     (Baltimore, MD) vol 1 (Vienna: IAEA) p 73
[38] Isler R.C. *et al* 1983 *Appl. Phys. Lett.* **42** 355
[39] Brau K. *et al* 1983 *Nucl. Fusion* **23** 1643
[40] Hawkes N.C. and Peacock N.J. 1985 *Nucl. Fusion* **25** 971
[41] Bitter M. *et al* 1985 *Phys. Rev.* A **32** 3011
[42] Isler R.C. *et al* 1986 *Nucl. Fusion* **26** 391
[43] Mattioli M. *et al* 1988 *J. Appl. Phys.* **64** 3345
[44] Weisen H. *et al* 1989 *Nucl. Fusion* **29** 2187
[45] Yoshida M. *et al* 2007 *Nucl. Fusion* **47** 856
[46] Politzer P.A. *et al* 2008 *Nucl. Fusion* **48** 075001
[47] Burrell K. *et al* 2009 *Phys. Rev. Lett.* **102** 155003
[48] Yoshida M. *et al* 2009 *Fusion Eng. Des.* **84** 2206
[49] Zastrow K.-D. *et al* 1998 *Nucl. Fusion* **38** 257
[50] deGrassie J.S. *et al* 2006 *Phys. Plasmas* **13** 112507
[51] Ono M. 1993 *Phys. Fluids* B **5** 241
[52] Eriksson L.-G. *et al* 2009 *Plasma Phys. Control. Fusion*
     51 044008
[53] Noterdaeme J.-M. *et al* 2003 *Nucl. Fusion* **43** 274
[54] LeBlanc B.P. *et al* 1999 *Phys. Rev. Lett.* **82** 331
[55] Eriksson L.-G. *et al* 2004 *Phys. Rev. Lett.* **92** 235001
[56] Lin Y. *et al* 2008 *Phys. Rev. Lett.* **101** 235002
[57] Lin Y. *et al* 2009 *Phys. Plasmas* **16** 056102
[58] Lin Y. *et al* 2011 *Nucl. Fusion* **51** 063002
[59] Lin Y. *et al* 2012 *Plasma Phys. Control. Fusion* **54** 074001
[60] Jaeger E.F. *et al* 2003 *Phys. Rev. Lett.* **90** 195001
[61] Perkins F.W. *et al* 2001 *Phys. Plasmas* **8** 2181
[62] Idei H. *et al* 1993 *Phys. Rev. Lett.* **71** 2220
[63] Sakamoto Y. *et al* 2006 *Plasma Phys. Control. Fusion* **48** A63
[64] Yoshida M. *et al* 2009 *Phys. Rev. Lett.* **103** 065003
[65] Kim J. *et al* 1994 *Phys. Rev. Lett.* **72** 2199
[66] Solomon W.M. *et al* 2006 *Phys. Plasmas* **13** 056116
[67] Ida K. *et al* 2001 *Phys. Rev. Lett.* **86** 5297
[68] Ida K. 1998 *Plasma Phys. Control. Fusion* **40** 1429
[69] Kamiya K. *et al* 2013 *Nucl. Fusion* **53** 013003
[70] Crombé K. *et al* 2005 *Phys. Rev. Lett.* **95** 155003
[71] Kamiya K. *et al* 2010 *Phys. Rev. Lett.* **105** 045004
[72] Grierson B.A. *et al* 2013 *Nucl. Fusion* **53** 063010
[73] Scott S.D. *et al* 1985 *Nucl. Fusion* **25** 359
[74] deVries P.C. *et al* 2010 *Plasma Phys. Control. Fusion*
     52 065004
[75] Fenzi C. *et al* 2011 *Nucl. Fusion* **51** 103038
[76] Yoshida M. *et al* 2006 *Plasma Phys. Control. Fusion* **48** 1673
[77] Ida K. *et al* 1991 *Phys. Rev. Lett.* **67** 58
[78] Ida K. *et al* 1997 *Phys. Plasmas* **4** 310
[79] Garofalo A.M. *et al* 2007 *Nucl. Fusion* **47** 1121
[80] Park J.K. *et al* 2009 *Phys. Rev. Lett.* **102** 065002
[81] Park J.K. *et al* 2009 *Phys. Plasmas* **16** 056115
[82] Garofalo A.M. *et al* 2009 *Phys. Plasmas* **16** 056119
[83] Sun Y. *et al* 2010 *Plasma Phys. Control. Fusion* **52** 105007
[84] Schaffer M.J. *et al* 2011 *Nucl. Fusion* **51** 103028
[85] Lazzaro E. *et al* 2002 *Phys. Plasmas* **9** 3906
[86] LaHaye R.J. *et al* 1994 *Phys. Plasmas* **1** 373
[87] Garofalo A.M. *et al* 2008 *Phys. Rev. Lett.* **101** 195005
[88] Zhu W. *et al* 2006 *Phys. Rev. Lett.* **96** 225002
[89] Callen J.D. 2011 *Nucl. Fusion* **51** 094026
[90] Cole A.J. *et al* 2011 *Phys. Rev. Lett.* **106** 225002
[91] Versloot T.W. *et al* 2010 *Plasma Phys. Control. Fusion*
     52 045014
[92] Versloot T.W. *et al* 2011 *Plasma Phys. Control. Fusion*
     53 065017
[93] Sugama H. and Horton W. 1997 *Phys. Plasmas* **4** 405
[94] Garbet X. *et al* 2012 *Plasma Phys. Control. Fusion*
     54 055007
[95] Rice J.E. *et al* 2007 *Fusion Sci. Technol.* **51** 288
[96] Bell M.G. 1979 *Nucl. Fusion* **19** 33
[97] Kostek C.A. *et al* 1983 *Plasma Phys.* **25** 421
[98] Bugarya V.I. *et al* 1985 *Nucl. Fusion* **25** 1707
[99] Duval B.P. *et al* 1992 *Nucl. Fusion* **32** 1405
[100] Rice J.E. *et al* 1997 *Nucl. Fusion* **37** 421
[101] Scarabosio A. *et al* 2006 *Plasma Phys. Control. Fusion*
     48 663
[102] Duval B.P. *et al* 2007 *Plasma Phys. Control. Fusion* **49** B195
[103] Duval B.P. *et al* 2008 *Phys. Plasmas* **15** 056113
[104] Ida K. *et al* 1991 *Nucl. Fusion* **31** 943
[105] Romannikov A. *et al* 2000 *Nucl. Fusion* **40** 319
[106] deVries P.C. *et al* 2008 *Nucl. Fusion* **48** 035007
[107] Trier E. *et al* 2008 *Nucl. Fusion* **48** 092001
[108] Crombé K. *et al* 2009 *Plasma Phys. Control. Fusion*
     51 055005
[109] deGrassie J.S. *et al* 2009 *Nucl. Fusion* **49** 085020
[110] Koide Y. *et al* 1993 *Proc. 14th Int. Conf. on Plasma Physics*
     and Controlled Nuclear Fusion Research (Wurzburg,
     Germany) vol 1 (Vienna: IAEA) p 777
[111] Platz P. *et al* 1995 *22nd European Physical Society Conf. on*
     Plasma Physics and Controlled Fusion (Bournemouth,
     UK, 2–7 July 1995) vol 19C, p III-337
[112] Ince-Cushman A. *et al* 2009 *Phys. Rev. Lett.* **102** 035002
[113] Rice J.E. *et al* 2009 *Nucl. Fusion* **49** 025004
[114] Shi Y. *et al* 2011 *Phys. Rev. Lett.* **106** 235001
[115] Rice J.E. *et al* 2013 *Nucl. Fusion* **53** 093015
[116] Rice J.E. *et al* 2013 *Phys. Rev. Lett.* **111** 125003
[117] Eriksson L.-G. *et al* 1992 *Plasma Phys. Control. Fusion*
     34 863
[118] Coffey I.H. *et al* 1996 *Proc. 11th Colloquium on UV and*
     X-Ray Spectroscopy of Astrophysical and Laboratory
     Plasmas (Nagoya, Japan, 1995) (*Frontiers Science Series*
     no 15) ed K. Yamashita and T. Watanabe (Tokyo, Japan:
     Universal Academy Press) p 431
[119] Eriksson L.-G. *et al* 1997 *Plasma Phys. Control. Fusion* **39** 27
[120] Rice J.E. *et al* 1998 *Nucl. Fusion* **38** 75
[121] Rice J.E. *et al* 1999 *Nucl. Fusion* **39** 1175
[122] Hoang G.T. *et al* 2000 *Nucl. Fusion* **40** 913
[123] Hutchinson I.H. *et al* 2000 *Phys. Rev. Lett.* **84** 3330
[124] Rice J.E. *et al* 2000 *Phys. Plasmas* **7** 1825
[125] Eriksson L.-G. *et al* 2001 *Nucl. Fusion* **41** 91
[126] Assas S. *et al* 2003 Toroidal plasma rotation in ICRF heated
     Tore Supra discharges *30th European Physical Society*
     Conf. on Plasma Physics and Controlled Fusion (St.
     Petersburg, Russia, 7–11 July 2003) vol 27A (ECA)
     P-I.138
[127] Rice J.E. *et al* 2004 *Phys. Plasmas* **11** 2427
[128] deGrassie J.S. *et al* 2004 *Phys. Plasmas* **11** 4323
[129] deGrassie J.S. *et al* 2007 *Phys. Plasmas* **14** 056115
[130] Yoshinuma M. *et al* 2009 *Nucl. Fusion* **49** 075036
[131] Solomon W.M. *et al* 2010 *Phys. Plasmas* **17** 056108
[132] Nave M.F.F. *et al* 2012 *Plasma Phys. Control. Fusion*
     54 074006
[133] Rice J.E. *et al* 2002 *Nucl. Fusion* **42** 510

[134] Rice J.E. *et al* 2003 *Nucl. Fusion* **43** 781
[135] Fiore C.L. *et al* 2010 *Nucl. Fusion* **50** 064008
[136] deGrassie J.S. *et al* 2003 *Nucl. Fusion* **43** 142
[137] Nishijima D. *et al* 2005 *Plasma Phys. Control. Fusion* **47** 89
[138] Tala T. *et al* 2007 *Nucl. Fusion* **47** 1012
[139] Tala T. *et al* 2007 *Plasma Phys. Control. Fusion* **49** B291
[140] deVries P.C. *et al* 2008 *Nucl. Fusion* **48** 065006
[141] Scott S.D. *et al* 1990 *Phys. Rev. Lett.* **64** 531
[142] deVries P.C. *et al* 2006 *Plasma Phys. Control. Fusion* **48** 1693
[143] Kallenbach A. *et al* 1991 *Plasma Phys. Control. Fusion* **33** 595
[144] Asakura N. *et al* 1993 *Nucl. Fusion* **33** 1165
[145] Hahm T.S. *et al* 2007 *Phys. Plasmas* **14** 072302
[146] Peeters A.G. *et al* 2009 *Phys. Plasmas* **16** 034703
[147] Lee W.D. *et al* 2003 *Phys. Rev. Lett.* **91** 205003
[148] Rice J.E. *et al* 2004 *Nucl. Fusion* **44** 379
[149] Reimerdes H. *et al* 2007 *Phys. Rev. Lett.* **98** 055001
[150] Sabbagh S.A. 2006 *Nucl. Fusion* **46** 635
[151] Solomon W.M. *et al* 2008 *Phys. Rev. Lett.* **101** 065004
[152] Tala T. *et al* 2009 *Phys. Rev. Lett.* **102** 075001
[153] Tardini G. *et al* 2009 *Nucl. Fusion* **49** 085010
[154] Mantica P. *et al* 2010 *Phys. Plasmas* **17** 092505
[155] Tala T. *et al* 2011 *Nucl. Fusion* **51** 123002
[156] Kaye S.M. *et al* 2009 *Nucl. Fusion* **49** 045010
[157] Yoshida M. *et al* 2008 *Plasma Fusion Res.* **3** S1007
[158] Yoshida M. *et al* 2009 *Nucl. Fusion* **49** 115028
[159] Nagashima K. *et al* 1994 *Nucl. Fusion* **34** 449
[160] Yoshida M. *et al* 2008 *Phys. Rev. Lett.* **100** 105002
[161] Gürcan O.D., Diamond P.H. and Hahm T.S. 2008 *Phys. Rev. Lett.* **100** 135001
[162] Peeters A.G. *et al* 2007 *Phys. Rev. Lett.* **98** 265003
[163] Weisen H. *et al* 2012 *Nucl. Fusion* **52** 042001
[164] Diamond P.H. *et al* 1995 *Proc. 15th Int. Conf. on Plasma Physics and Controlled Nuclear Fusion Research (Seville, Spain, 1994)* vol 3 (Vienna: IAEA) p 323
[165] Garbet X. *et al* 2002 *Phys. Plasmas* **9** 3893
[166] Peeters A.G. and Angioni C. 2005 *Phys. Plasmas* **12** 072515
[167] McDermott R.M. *et al* 2011 *Plasma Phys. Control. Fusion* **53** 035007
[168] McDermott R.M. *et al* 2011 *Plasma Phys. Control. Fusion* **53** 124013
[169] Solomon W.M. *et al* 2009 *Nucl. Fusion* **49** 085005
[170] Nagaoka K. *et al* 2011 *Nucl. Fusion* **51** 083022
[171] Hidalgo C. *et al* 1999 *Phys. Rev. Lett.* **83** 2203
[172] Hidalgo C. *et al* 2000 *Plasma Phys. Control. Fusion* **42** A153
[173] Ida K. *et al* 1995 *Phys. Rev. Lett.* **74** 1990
[174] Yoshida M. *et al* 2012 *Nucl. Fusion* **52** 023024
[175] Ida K. *et al* 1998 *J. Phys. Soc. Japan* **67** 4089
[176] Rice J.E. *et al* 2001 *Nucl. Fusion* **41** 277
[177] Solomon W.M. *et al* 2007 *Plasma Phys. Control. Fusion* **49** B313
[178] Ida K. *et al* 2010 *Nucl. Fusion* **50** 064007
[179] Goncalves B. *et al* 2006 *Phys. Rev. Lett.* **96** 145001
[180] Tala T.J.J. *et al* 2001 *Plasma Phys. Control. Fusion* **43** 507
[181] Ide S. *et al* 2004 *Nucl. Fusion* **44** 87
[182] Ernst D.R. *et al* 1998 *Phys. Plasmas* **5** 665
[183] Baylor L.R. *et al* 2004 *Phys. Plasmas* **11** 3100
[184] Grierson B.A. *et al* 2012 *Phys. Plasmas* **19** 056107
[185] Sakamoto Y. *et al* 2001 *Nucl. Fusion* **41** 865
[186] Rice J.E. *et al* 2011 *Phys. Rev. Lett.* **106** 215001
[187] Ku S. *et al* 2012 *Nucl. Fusion* **52** 063013
[188] Wang W.X. *et al* 2011 *Phys. Plasmas* **18** 042502
[189] Gürcan O.D. *et al* 2007 *Phys. Plasmas* **14** 042306
[190] Kwon J.M. *et al* 2012 *Nucl. Fusion* **52** 013004
[191] Gürcan O.D. *et al* 2010 *Phys. Plasmas* **17** 112309
[192] Camenen Y. *et al* 2009 *Phys. Rev. Lett.* **102** 125001
[193] Müller S.H. *et al* 2011 *Phys. Rev. Lett.* **106** 115001
[194] Rice J.E. *et al* 2005 *Nucl. Fusion* **45** 251
[195] Rice J.E. *et al* 2008 *Plasma Phys. Control. Fusion* **50** 124042
[196] LaBombard B. *et al* 2004 *Nucl. Fusion* **44** 1047
[197] Stoltzfus-Dueck T. *et al* 2012 *Phys. Rev. Lett.* **108** 065002
[198] Stacey W.M. 2011 *Phys. Plasmas* **18** 102504
[199] Stacey W.M. 2011 *Phys. Plasmas* **18** 122504
[200] Chang C.S. and Ku S. 2008 *Phys. Plasmas* **15** 062510
[201] deGrassie J.S. *et al* 2012 *Nucl. Fusion* **52** 013010
[202] Bortolon A. *et al* 2006 *Phys. Rev. Lett.* **97** 235003
[203] Rice J.E. *et al* 2011 *Nucl. Fusion* **51** 083005
[204] Rice J.E. *et al* 2012 *Phys. Plasmas* **19** 056106
[205] Angioni C. *et al* 2011 *Phys. Rev. Lett.* **107** 215003
[206] McDevitt C.J. *et al* 2009 *Phys. Rev. Lett.* **103** 205003
[207] Wang L. *et al* 2013 *Phys. Rev. Lett.* **110** 265006
[208] Ida K. *et al* 2001 *Phys. Rev. Lett.* **86** 3040
[209] Ida K. *et al* 2002 *Plasma Phys. Control. Fusion* **44** 361
[210] Nagaoka K. *et al* 2013 *Phys. Plasmas* **20** 056116
[211] Reinke M.L. *et al* 2013 *Plasma Phys. Control. Fusion* **55** 012001
[212] Shi Y.J. *et al* 2013 *Nucl. Fusion* **53** 113031
[213] White A.E. *et al* 2013 *Phys. Plasmas* **20** 056106
[214] Ida K. *et al* 2013 *Phys. Rev. Lett.* **111** 055001
[215] Kim S.S. *et al* 2011 *Nucl. Fusion* **51** 073021
[216] Luce T.C. *et al* 1992 *Phys. Rev. Lett.* **68** 52
[217] Mantica P. *et al* 2000 *Phys. Rev. Lett.* **85** 4534
[218] Rice J.E. *et al* 2013 *Nucl. Fusion* **53** 033004
[219] Gentle K.W. *et al* 1995 *Phys. Rev. Lett.* **74** 3620
[220] Mantica P. *et al* 1999 *Phys. Rev. Lett.* **82** 5048
[221] Inagaki S. *et al* 2006 *Plasma Phys. Control. Fusion* **48** A251
[222] Ida K. *et al* 2008 *Phys. Rev. Lett.* **101** 055003
[223] Dif-Pradalier G. *et al* 2010 *Phys. Rev.* E **82** 025401
[224] Rice J.E. *et al* 2011 *Phys. Rev. Lett.* **107** 265001
[225] Rice J.E. *et al* 2007 *Nucl. Fusion* **47** 1618
[226] Solomon W.M. *et al* 2011 *Nucl. Fusion* **51** 073010